THE ASTROPHYSICAL JOURNAL, 411:153–169, 1993 July 1

DYNAMICALLY HOT GALAXIES. II. GLOBAL STELLAR POPULATIONS

RALF BENDER
Landessternwarte Königstuhl, D6900 Heidelberg, Germany
DAVID BURSTEIN
Department of Physics and Astronomy, Arizona State University, Tempe, AZ 85287-1504
AND
S. M. FABER
UCO/Lick Observatory, University of California, Santa Cruz, CA 95064
Received 1992 August 31; accepted 1992 December 31

ABSTRACT

The global relationship between the stellar populations and structural properties of hot galaxies is studied using the same sample of objects analyzed in Bender, Burstein, and Faber. Two measures of global stellar population are used: the Mg_2 index at the center of a galaxy and $(B-V)_0$ color measured over a much larger volume. The sample of galaxies studied includes luminous ellipticals that span a wide range in luminosity, compact ellipticals, dwarf ellipticals, and the bulges of S0 galaxies. The degree of anisotropy of internal stellar motions is known for most of these objects.

The total sample spans a range of over four orders of magnitude in mass and surface brightness, and the various subclasses populate the fundamental plane in very different ways. Despite this, all galaxies follow the *same mean* relationship between Mg_2 and velocity dispersion σ_0. The relative tightness of this relation is impressive: galaxies show a mean scatter of only 0.025 mag in Mg_2, versus a full range of nearly 0.35 mag in Mg_2. At least some of the scatter is intrinsic, but the residuals do not correlate with any of the structural properties studied (e.g., velocity anisotropy; effective radius, surface brightness or mass). The residuals also do not show any relation with the positions of the objects within *or* perpendicular to the fundamental plane. The only properties that do correlate are the morphological and kinematical peculiarities of a handful of disturbed ellipticals, as shown both in this paper and in the study of Schweizer et al. The observed scatter sets an upper limit of 15% on the rms variation of both age and metallicity at fixed σ_0 for bright ellipticals.

The Mg_2–$(B-V)_0$ relation is also examined and found to be tight and consistent for all dynamically hot galaxies. Several S0 galaxies have much bluer *global* colors compared to *central* Mg_2 than do other hot galaxies, but these exceptions are likely due to contamination of the global color by young disk light. The generally tight relation between *central* Mg_2 and *global* $(B-V)_0$ means that variations in the internal color and line-strength gradients from galaxy to galaxy must be small.

The Mg_2–σ_0 relationship can be reformulated as a function of the mass of the galaxy $\boldsymbol{M}$ and the *average* volume density of baryonic matter ρ as defined by the stars. This new relation can be expressed as $Mg_2 = (\boldsymbol{M}^2\rho)^{0.033}$. Though ρ is used here to denote average volume density, this relation might also be interpreted as a correlation between the local stellar population and local volume density *within* each dynamically hot galaxy. This prediction will be tested against observed color and line strength gradients in the next paper of this series.

Subject headings: galaxies: abundances — galaxies: photometry — galaxies: stellar content

1. INTRODUCTION

In the first paper of this series (Bender, Burstein, & Faber 1992, hereafter B^{2}F1), we initiated a study of the structural properties of "dynamically hot galaxies" (DHGs) by investigating their distribution in the fundamental plane defined by central velocity dispersion (σ_0), effective radius (r_e) and effective surface brightness (SB_e). In the present paper we extend this study to a key global property of galaxies that was purposefully omitted from the first paper—the stellar populations of these galaxies. As will be demonstrated here, we have found that the connection between the global stellar population of a DHG and its global structural properties is, to first order, exceedingly simple: Only the central velocity dispersion appears to play a strong role in determining the stellar population. Surprisingly, the wide variety of sizes, surface brightnesses, and masses of the DHGs appear to be of insignificant secondary influence on their resident stellar populations.

As in B^{2}F1, our sample of DHGs includes giant ellipticals, ellipticals of intermediate luminosity, bulges of S0 and Sa galaxies, compact ellipticals, bright dwarf ellipticals and dwarf spheroidals. The degree of velocity dispersion anisotropy is known for most galaxies in this sample. This core sample is augmented by ellipticals observed by the "7 Samurai" (Burstein et al. 1987; Davies et al. 1987; Faber et al. 1989), for which no information on velocity anisotropy is currently available.

In B^{2}F1 we parameterized the physical properties that define the fundamental plane in terms of an orthogonal coordinate system (termed κ-space) that permitted us to better visualize the physical processes that determine the distribution of galaxies both within, and perpendicular to, this plane. The κ coordinates are an orthogonal transformation from the original set of σ_0, r_e, and SB_e: κ_1 is proportional to log mass; κ_2 involves a linear combination of both log surface brightness and log M/L; and κ_3 is proportional to log M/L.

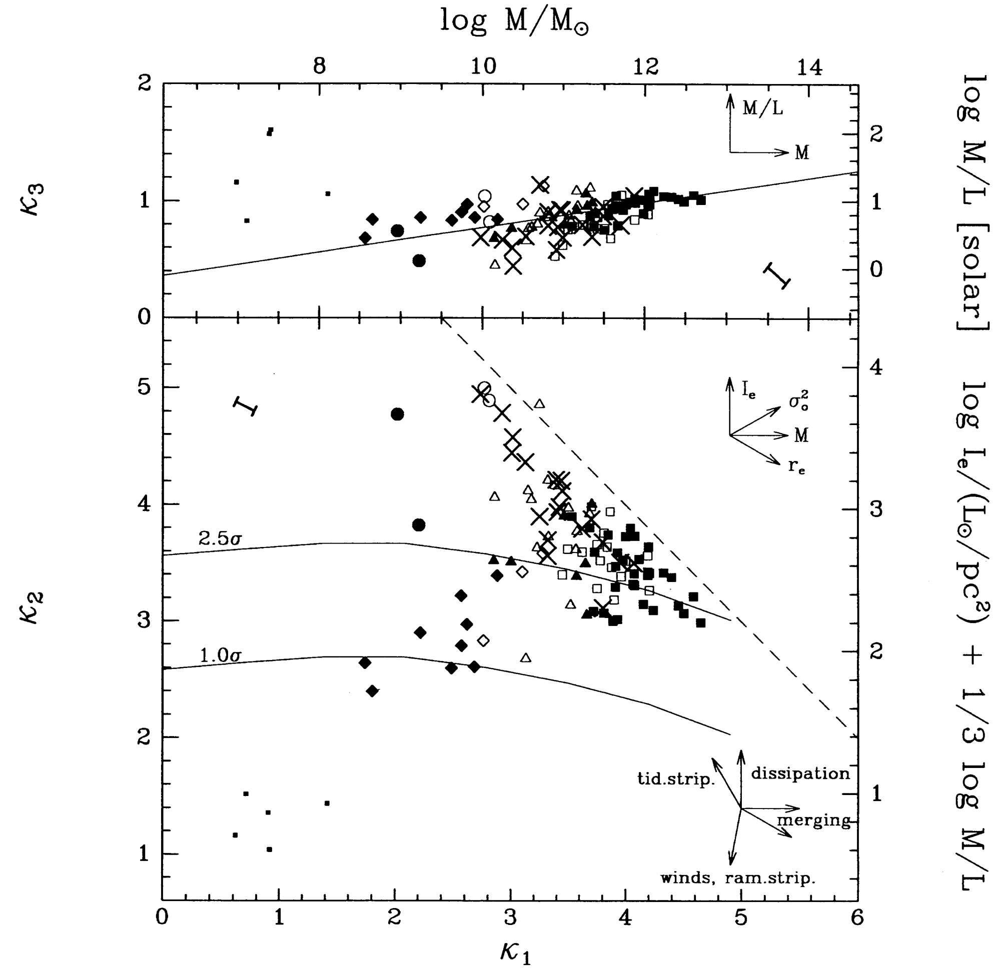

FIG. 1.—Distribution of all types of dynamically hot galaxies (DHGs) in κ-space. The κ_1-κ_2 plane shows the DHG fundamental plane face-on, κ_1-κ_3 is an edge-on view. Values of the corresponding physical parameters are given on the opposite sides of the figures (masses M were determined from $M = 5G^{-1}\sigma_0^2 r_e$ and are given in solar units; mean effective surface brightnesses $\langle I \rangle_e$ were derived from $\log \langle I \rangle_e = -0.4(SB_e - 27)$ and refer to units of $L_\odot$ pc^{-2}. Squares denote giant ellipticals (absolute magnitudes $M_T < -20.5$ mag), triangles denote ellipticals of intermediate luminosity (-20.5 mag $< M_T < -18.5$ mag), circles denote compact galaxies, and diamonds denote dwarf galaxies with known kinematics. Open symbols are galaxies that are rotationally flattened; filled symbols are galaxies that have anisotropic kinematics. Bulges are represented by only one symbol (*crosses;* all those measured appear to be rotationally flattened, B^{2}F1). The five small filled squares refer to Fornax (which is anisotropic) and four other dwarf spheroidal companions of the Galaxy, for which no spatially resolved kinematics are available. The arrows in the upper right indicate the directions in which the basic global parameters of DHGs increase. The arrows in the lower right of the lower panel sketch how the major processes move objects in the plane (tid.strip = tidal stripping, ram.strip = ram pressure stripping). Horizontal lines in the lower diagram represent κ_1-κ_2 loci for galaxies of different mass arising from a CDM density fluctuation spectrum with 1.0 σ and 2.5 σ overdensity and a constant amount of dissipation in the baryonic component. Vertical normalizaton is arbitrary. The small thick error bars indicate the influence of a distance error of $\pm 30\%$. For detailed discussion of this figure, please see B^{2}F1.

Figure 1, taken from B^{2}F1, shows the distribution of DHGs both within and perpendicular to the fundamental plane, as defined by the κ coordinate system. Each type of DHG is assigned a unique plotting symbol, as explained in the figure caption and in § 2. Symbols denote both the kind of DHG and the degree of anisotropy of the stellar motions.

As discussed in B^{2}F1, DHGs appear to populate two main sequences within the fundamental plane. The first consists of normal luminous ellipticals, compact ellipticals and bulges and is visible as the cloud of points to the upper right in Figure 1*b*, bounded above by the diagonal line. Within this sequence, brighter objects have lower surface brightness and are supported mainly by anisotropic velocity dispersions, whereas fainter objects have higher surface brightness and are largely isotropic rotators. We suggested in B^{2}F1 that these trends are consistent with a merger picture for the origin of this sequence, with mergers that are progressively more stellar, less gaseous, and less dissipative at higher masses—hence the proposed name "gas/stellar (or GS) continuum."

The second sequence is nearly perpendicular to the first and consists purely of objects usually termed "dwarfs." It can be seen running diagonally to the lower left of the GS continuum in Figure 1*b*. Unlike galaxies in the GS continuum, brighter objects in the dwarf sequence have higher surface brightnesses, not lower, and the entire sequence appears to be composed of anisotropic galaxies. Because of these differences, B^{2}F1 concluded that the dwarf sequence must have formed differently from the GS continuum, most likely involving some form of substantial gas loss.

All DHGs except extreme dwarf spheroidals lie near the fundamental plane defined by the luminous ellipticals (Fig. 1*a*). This indicates that a relatively tight relation exists between mass-to-light ratio and mass for all these systems. Somewhat brighter dwarf ellipticals lie $\sim$0.1 dex above the plane, while

bulges tend to scatter ~0.1 dex below the plane. These relationships are discussed in detail in B^{2}F1.

Relevant data concerning the global stellar populations of luminous ellipticals can be summarized as follows:

1. Most studies indicate that the stellar populations of bright ellipticals are basically "old," although there is general disagreement on what the term "old" means exactly, or even whether all bright ellipticals are of the same age (O'Connell 1980; Burstein et al. 1984; Rose 1985; Renzini 1986; Faber, Worthey, & Gonzalez 1992).

2. More luminous ellipticals are redder and have stronger metal absorption lines than less luminous ones (Faber 1973; Sandage & Visvanathan 1978). The absorption index Mg_2 has been empirically found to measure accurately small differences among old stellar populations (Burstein et al. 1984) and to increase markedly in elliptical galaxies with increasing luminosity and velocity dispersion (e.g., Burstein et al. 1988b).

3. Studies of colors and absorption line indices strongly suggest that differences in metallicity are the dominant source of their variation of among DHGs of different absolute luminosities (e.g., Faber 1973), though age may also play some role (Schweizer et al. 1990). Differences from solar abundance ratios have also been suggested by several studies (e.g., Burstein 1985; Faber et al. 1992).

4. Intrinsic scatter exists in the Mg_2–σ_0 relation for luminous ellipticals (Burstein et al. 1988b). In at least one sample of galaxies, the dispersion of Mg_2 on σ_0 is correlated with the degree of disturbance in the optical appearance of the galaxy (Schweizer et al. 1990). As with point (3) above, this intrinsic dispersion can be interpreted as a combination of age and/or metallicity differences among ellipticals with similar luminosities.

5. Metallicity gradients (as inferred from color gradients) within elliptical galaxies appear to be roughly correlated with local escape velocity within a galaxy (Franx & Illingworth 1990). However, color and line strength gradients are not precisely identical even among ellipticals of similar absolute luminosity (Thomsen & Baum 1989; Gorgas, Efstathiou, & Aragon Salamanca 1990; Efstathiou & Gorgas 1985) and show evidence for sub-structure (Bender & Surma 1992). It is furthermore not clear how to decompose an individual gradient into separate age and metallicity effects.

The available data on the stellar populations of fainter DHGs are much less owing to their relative faintness. Very little is known about stars in bulges generally, although detailed studies have been made of the Galactic bulge (Frogel 1988; Terndrup 1988) and the bulge of M31 (Rich & Mould 1991). Detailed information is available for the dwarf spheroidal and bright dwarf elliptical companions of the Galaxy and M31, and for the nearby compact elliptical M32, in the form of color-magnitude diagrams for the brighter stars (Freedman 1992). For these objects the following results have been obtained:

6. As for bright ellipticals, the metal abundance of dwarf spheroidals has been found to increase with luminosity, with a slope that is probably similar to the one observed for giant ellipticals, but a zero point that has been claimed to be different (Aaronson & Mould 1985).

7. The color-magnitude diagrams of most dwarf spheroidals in the Local Group show direct evidence for intermediate age stars, indicating that star formation ceased only a few Gyr ago (Aaronson & Mould 1985; Freedman 1992). M32, structurally more similar to bulges of S0's than to dwarfs (see Fig. 1), also shows evidence that the bulk of its stars are of intermediate age (5 Gyr; O'Connell 1980; Burstein et al. 1984; Freedman 1992). Yet M32 lies on an extension of the Mg_2–σ_0 relation for brighter ellipticals (Burstein et al. 1988b) and is well-known to be spectroscopically indistinguishable from many other low-luminosity ellipticals. This suggests that other low-luminosity ellipticals might also be dominated by stellar populations that are young relative to Galactic globular clusters.

Given the clear physical differences between the dwarf and GS sequences, it is obviously important to understand how their stellar populations are related. In this paper we are concerned only with the *global* stellar populations of dynamically hot galaxies. We confine ourselves to the central Mg_2 index and the global $B-V$ color because these are the only two measures of stellar populations that are available for a large number of objects and, even more important, are those which have been measured with the highest signal-to-noise ratios. While it is of interest to see how other measures of stellar populations (e.g., Fe-line measurements) fare in the kinds of comparisons made here, that is beyond the scope of the present paper. Gradients of stellar populations *within* galaxies are also a separate issue and will be covered in Paper III (in preparation). The basic data used in this paper are presented in § 2. The fundamental global correlation between stellar population [represented by Mg_2 and $(B-V)_0$] and velocity dispersion is presented in § 3, together with a discussion of the possible sources of scatter. A possible extension of this correlation *among* galaxies to gradients *within* galaxies is developed in § 4 and will be further explored in Paper III. In § 5 we summarize our conclusions.

2. DATA

The primary data sample for this paper includes all galaxies from B^{2}F1 that have measures of line strengths either directly on the Mg_2 system or calibrated to this system. The data include: 48 bright luminous ellipticals, $M_T < -20.5$ (*denoted by large squares in all figures*); 20 ellipticals of intermediate luminosity, $-18.5 > M_T \geq -20.5$ (*large triangles*); four NGC 4486B-type compact ellipticals (*large circles*); 25 bulges of S0 and Sa galaxies, of all luminosities (*crosses*; these are six more than the bulges used in B^{2}F1); 12 bright dwarf ellipticals, $-14 \geq M_T > -18.5$ (*diamonds*); and five faint dwarf spheroidals, $M_T > -14$ (*small closed squares*). The larger 7 Samurai data set, for which anisotropies are not measured, are plotted as small open squares. Most galaxies in the primary sample are also distinguished by the degree of anisotropy in their internal velocity dispersions, as measured by the parameter $(v/\sigma_0)^*$ and discussed in detail in B^{2}F1. If $(v/\sigma_0)^* < 0.7$ the galaxy is classed as anisotropic, and the data are plotted as large filled symbols; if $(v/\sigma_0)^* \geq 0.7$, the galaxy is classed as isotropic, and the data are plotted as large open symbols. No velocity anisotropy measures are available for the faint dwarf spheroidals (except for the Fornax dwarf), or for the supplemental 7 Samurai data.

The basic data base was compiled partially from the literature and partially from observations described below. These data are summarized here and listed in Table 1. Detailed references to the literature are also given in Table 1:

1. Central Mg_2 values and velocity dispersions for luminous elliptical galaxies were taken from the 7 Samurai sample (Faber et al. 1989).

2. Metallicities of dwarf spheroidals in the Local Group were taken from Aaronson & Mould (1985) and Caldwell et al. (1992) and references therein. To place these metallicities on

TABLE 1

OBSERVED PHYSICAL AND STELLAR POPULATION PROPERTIES OF DYNAMICALLY HOT GALAXIES

Name (1)	l (2)	b (3)	Type (4)	Distance (Mpc) (5)	Source (6)	$\log \sigma_0$ (km s^{-1}) (7)	Source (8)	$\log r_e$ (kpc) (9)	SB_e (mag arcsec^{-2}) (10)	M_T (11)	Source (12)	A_B (13)	$\log (v/\sigma_0)^*$ (14)	Mg_2 (15)	Source (16)	$(B-V)_0$ (17)	Source (18)	a_4 (19)
									Giant Ellipticals									
N315	124°.6	−32°.5	LA	107.2	1	2.546	1	1.486	22.36	−23.61	1	0.26	−1.046	0.283	1	1.00	1	−0.31
N584	149.8	−67.6	E4	39.6	1	2.337	1	0.724	20.44	−21.72	1	0.13	0.190	0.283	1	0.93	1	1.50
N636	155.1	−67.4	E3	39.6	1	2.194	1	0.562	20.71	−20.65	1	0.11	0.017	0.273	1	0.92	1	0.80
N720	173.0	−70.4	E5	35.8	2	2.392	1	0.840	21.14	−21.60	1	0.00	−0.638	0.330	1	0.99	1	...
N777	139.7	−29.2	E1	99.4	1	2.542	1	1.134	21.60	−22.61	1	0.15	−0.558	0.325	1	0.99	1	−0.20
N821	151.6	−47.6	E6	37.7	2	2.298	1	0.922	21.85	−21.31	1	0.16	−0.155	0.304	1	0.94	1	2.50
N1052	182.0	−57.9	E4	29.3	1	2.313	1	0.723	21.11	−21.05	1	0.06	0.000	0.316	1	0.99	1	...
N1395	216.2	−52.1	E2	31.0	1	2.412	1	0.836	21.22	−21.50	1	0.01	0.041	0.313	1	0.97	1	...
N1399	236.7	−53.6	E1	26.4	1	2.491	1	0.737	20.68	−21.55	1	0.00	−0.602	0.334	1	0.99	1	0.00
N1404	236.9	−53.6	E1	26.4	1	2.353	1	0.537	20.02	−21.21	1	0.00	−0.013	0.317	1	0.97	1	0.50
N1407	209.6	−50.4	E0	31.0	1	2.455	1	1.041	21.85	−21.90	1	0.16	−0.076	0.327	1	0.99	1	−0.20
N1549	265.4	−43.8	E0	19.6	1	2.312	1	0.658	20.96	−20.87	1	0.00	−0.180	0.346	1	0.95	1	−0.40
N1600	200.4	−33.2	E3	98.6	1	2.506	1	1.360	22.17	−23.17	1	0.08	−1.301	0.324	1	0.97	1	−1.20
N1700	203.7	27.6	E4	81.1	1	2.368	1	0.735	19.94	−22.28	1	0.12	−0.097	0.278	1	0.92	1	0.90
N2300	127.7	27.8	LA0	45.6	1	2.430	1	0.905	21.51	−21.56	1	0.22	−1.097	0.319	1	1.04	1	−0.60
N2974	239.5	35.0	E4	34.5	2	2.346	1	0.795	21.28	−21.24	1	0.11	0.188	0.300	1	0.99	1	0.50
N3091	268.8	27.5	E3	76.1	1	2.463	1	1.003	21.52	−22.04	1	0.14	−0.420	0.317	1	0.97	1	−0.60
N3557	281.6	21.1	E3	54.3	2	2.465	1	1.001	21.01	−22.54	1	0.55	0.041	0.307	1	0.97	1	−0.20
N3607	230.6	66.4	E1	20.4	1	2.394	1	0.816	21.61	−21.02	1	0.00	−0.036	0.303	1	0.96	1	...
N3610	143.5	54.5	E5	39.1	1	2.201	1	0.388	19.25	−21.23	1	0.00	0.041	0.257	1	0.82	1	2.50
N3613	144.3	55.1	E6	39.0	1	2.323	1	0.667	20.78	−21.10	1	0.00	−0.076	0.279	1	0.96	1	0.70
N3640	256.9	57.8	E3	27.0	1	2.246	1	0.639	20.82	−20.92	1	0.10	0.170	0.263	1	0.93	1	−0.20
N3904	287.0	31.7	E2	31.6	1	2.333	1	0.555	20.50	−20.82	1	0.18	−0.444	0.312	1	0.93	1	0.00
N4125	130.2	51.3	E6P	38.3	1	2.359	1	1.049	21.46	−22.33	1	0.03	−0.032	0.295	1	0.94	1	0.95
N4168	267.7	73.3	E2	43.8	2	2.259	1	0.987	22.23	−21.25	1	0.05	−0.589	0.260	1	0.87	1	...
N4261	281.8	67.4	E2	41.0	2	2.468	1	0.889	21.25	−21.74	1	0.00	−1.000	0.330	1	0.99	1	−1.30
N4365	283.8	69.2	E3	20.7	1	2.394	1	0.752	21.42	−20.88	1	0.00	−1.097	0.321	1	0.99	1	−1.10
N4374	278.2	74.5	E1	20.7	1	2.458	1	0.743	20.81	−21.45	1	0.13	−1.046	0.305	1	0.98	1	−0.40
N4406	279.1	74.6	E3	20.7	1	2.398	1	0.954	21.65	−21.66	1	0.11	−0.745	0.311	1	0.91	1	−0.70
N4472	286.9	70.2	E2	20.7	1	2.458	1	1.014	21.40	−22.21	1	0.00	−0.328	0.306	1	0.98	1	−0.30
N4494	228.6	85.3	E1	22.4	1	2.095	1	0.697	20.97	−21.06	1	0.06	0.093	0.275	1	0.90	1	0.30
N4589	124.2	42.9	E2	36.6	1	2.332	1	0.870	21.67	−21.22	1	0.04	−0.244	0.320	1	0.95	1	...
N4621	294.4	74.4	E5	20.7	1	2.381	1	0.673	20.98	−20.93	1	0.07	−0.092	0.328	1	0.99	1	1.50
N4636	297.8	65.5	E0	20.7	1	2.281	1	0.996	22.23	−21.29	1	0.01	−0.602	0.311	1	0.96	1	−0.10
N4649	295.9	74.3	E2	20.7	1	2.533	1	0.873	21.10	−21.81	1	0.04	−0.337	0.338	1	1.01	1	−0.50
N4697	301.7	57.1	E6	20.4	2	2.218	1	0.876	21.41	−21.51	1	0.04	−0.108	0.297	1	0.95	1	1.40
N4889	57.2	87.9	E4	137.9	1	2.581	1	1.326	21.96	−23.21	1	0.05	−1.320	0.359	1	1.04	1	−0.25
N5322	110.3	55.5	E3	42.1	1	2.350	1	0.861	20.82	−22.03	1	0.00	−0.585	0.276	1	0.89	1	−0.90
N5576	348.7	57.9	E3	30.4	1	2.272	1	0.458	20.18	−20.66	1	0.04	−0.658	0.253	1	0.90	1	−0.50
N5846	0.4	48.8	E0	31.9	1	2.444	1	1.110	22.25	−21.85	1	0.14	−0.986	0.321	1	0.99	1	0.00
N6411	89.7	32.6	E2	78.4	2	2.192	1	1.010	21.82	−21.78	1	0.14	−1.301	0.270	1	0.94	1	−0.30
N6909	352.8	−35.5	E6	56.0	1	2.172	1	0.924	21.84	−21.32	1	0.07	−0.538	0.208	1	0.86	1	−0.50
N7507	23.4	−68.0	E0	32.1	1	2.377	1	0.692	20.63	−21.38	1	0.20	−0.444	0.324	1	0.96	1	−0.10
N7619	87.7	−48.3	E2	74.3	1	2.528	1	1.067	21.53	−22.35	1	0.16	−0.276	0.336	1	1.01	1	0.20
N7626	87.9	−48.4	E1P	74.3	1	2.369	1	1.137	21.87	−22.36	1	0.16	−0.921	0.336	1	1.00	1	...
N7785	98.5	−54.3	E5	80.7	2	2.464	1	1.023	21.44	−22.22	1	0.17	−0.328	0.296	1	0.96	1	−1.50
I1459	4.7	−64.1	E3	33.1	1	2.488	1	0.796	20.81	−21.71	1	0.00	−0.658	0.321	1	0.99	1	...
I4296	313.5	28.0	E0	69.2	1	2.509	1	1.286	22.07	−22.90	1	0.12	−0.194	0.323	1	0.98	1	0.00

TABLE 1—*Continued*

Name (1)	l (2)	b (3)	Type (4)	Distance (Mpc) (5)	Source (6)	log σ_0 (km s^{-1}) (7)	Source (8)	log r_e (kpc) (9)	SB_e (mag arcsec^{-2}) (10)	M_T (11)	Source (12)	A_B (13)	log $(v/\sigma_0)^*$ (14)	Mg_2 (15)	Source (16)	$(B-V)_0$ (17)	Source (18)	a_4 (19)
Intermediate Ellipticals																		
N1379	236.7	−54.1	E0	27.4	1	2.125	1	0.738	21.79	−20.44	1	0.00	0.056	0.257	1	0.92	1	0.20
N1439	215.1	−50.4	E1	31.0	1	2.194	1	0.796	22.15	−20.38	1	0.07	−0.493	0.269	1	0.90	1	...
N2694	167.3	40.2	E1	89.2	1	2.176	4	0.110	19.70	−19.70	4	0.07	0.044	...	...	...	1	...
N3156	238.3	45.1	L	22.7	1	1.845	4	0.744	22.49	−19.77	4	0.04	0.058	0.149	1	0.72	1	...
N3193	213.0	54.9	E2	23.9	1	2.311	1	0.444	20.69	−20.08	1	0.08	−0.099	0.295	1	0.95	1	0.30
N3377	231.2	58.3	E5	13.2	1	2.116	1	0.341	20.76	−19.49	1	0.06	−0.142	0.270	1	0.90	1	0.50
N3379	233.5	57.6	E1	13.2	1	2.303	1	0.356	20.16	−20.17	1	0.05	−0.086	0.308	1	0.97	1	0.20
N3608	230.4	66.5	LAS0	20.4	1	2.310	1	0.547	21.41	−19.87	1	0.00	−0.353	0.312	1	0.97	1	−0.20
N3818	273.6	52.7	E5	25.7	2	2.314	1	0.427	21.19	−19.49	1	0.11	−0.031	0.315	1	0.92	1	2.30
N4278	193.8	82.8	E1	14.6	1	2.425	1	0.369	20.60	−19.79	1	0.10	−0.150	0.291	1	0.96	1	...
N4291	125.6	41.6	E2	36.7	1	2.413	1	0.420	20.25	−20.40	1	0.06	−0.284	0.308	1	0.96	1	−0.40
N4387	278.8	74.5	E5	20.7	1	1.922	1	0.193	20.80	−18.71	1	0.13	−0.156	0.240	1	0.92	1	−1.00
N4473	281.6	75.4	E5	20.7	1	2.250	1	0.405	20.19	−20.38	1	0.04	−0.398	0.304	1	0.96	1	0.90
N4478	283.4	74.4	E2	20.7	1	2.174	1	0.152	19.87	−19.44	1	0.09	−0.024	0.253	1	0.89	1	−0.80
N4551	288.2	74.7	E3	20.7	1	1.999	1	0.253	20.95	−18.86	1	0.12	−0.257	0.264	1	0.94	1	−0.70
N4564	289.6	73.9	E6	20.7	1	2.185	1	0.342	20.64	−19.61	1	0.04	0.023	0.321	1	0.96	1	2.20
N4660	296.8	74.0	E5	20.7	1	2.296	1	0.112	19.72	−19.39	1	0.00	0.016	0.297	1	0.98	1	2.70
N4742	303.1	52.4	E4	22.3	2	1.970	1	0.104	19.36	−19.71	1	0.09	0.209	0.177	1	0.79	1	0.41
N5831	359.4	49.0	E3	31.9	1	2.220	1	0.619	21.42	−20.22	1	0.13	−0.732	0.289	1	0.95	1	...
N5845	0.3	48.9	E3	31.9	1	2.400	1	−0.200	18.38	−19.17	2	0.14	−0.041	0.304	1	0.98	1	0.80
Bright Dwarf Ellipticals																		
N147	119.8	−14.3	dE5	0.7	3	1.369	2	−0.187	23.32	−14.60	3	0.71	−0.409	0.120	2	0.78	2	...
N185	120.8	−14.5	dE2	0.7	3	1.352	2	−0.237	22.60	−14.80	3	0.78	−1.000	0.080	2	0.73	2	...
N205	120.7	−21.1	dE5	0.7	3	1.623	2	−0.108	22.32	−15.60	3	0.17	−1.350	0.100	2	0.63	2	...
N3605	230.6	66.4	E4	20.4	1	2.078	1	0.236	21.42	−18.31	1	0.00	−0.132	0.213	1	0.87	1	−0.90
N3641	257.0	57.8	E1	27.0	1	2.217	4	0.209	21.32	−18.27	4	0.10	0.185	0.284	1	0.92	1	...
N4431	281.0	74.1	dS0N	20.7	1	1.830	5	0.250	22.60	−18.00	5	0.08	0.000	0.203	2	0.80	2	...
N4467	286.7	70.2	E2	20.7	1	1.826	4	−0.016	21.74	−16.72	4	0.00	−0.289	0.266	2	0.94	1	...
N4515	280.6	78.3	L	20.7	1	1.954	4	0.170	21.30	−18.49	4	0.03	−0.259	0.206	2	...	...	...
I794	281.8	74.0	dE3N	20.7	1	1.730	4	0.340	22.92	−17.50	4	0.05	−0.460	0.202	2	...	...	...
I3393	282.5	73.9	dE7N	20.7	1	1.740	5	0.160	22.62	−16.95	5	0.10	−0.300	0.167	2	...	...	...
U7436	272.8	75.9	dE5	20.7	1	1.650	5	0.220	22.90	−16.90	5	0.08	−0.350	0.164	2	...	...	...
V351	282.5	66.6	dE7	20.7	1	1.813	4	0.080	22.34	−16.70	4	0.00	−0.637	0.176	2	...	...	...
Compact Ellipticals																		
N0221	121.2	−22.0	cE2	0.7	3	1.903	3	−0.947	18.33	−15.70	3	0.31	−0.301	0.185	1	0.84	1	0.00
N4486B	283.4	74.6	cE0	20.7	1	2.301	4	−0.680	18.30	−17.40	4	0.09	−0.013	0.312	2	0.98	1	0.80
N5846A	0.4	48.8	cE2	31.9	1	2.230	4	−0.480	18.20	−18.49	4	0.14	−0.011	0.290	2	...	...	0.00
I0767	268.8	72.2	cE3	20.7	1	1.700	4	−0.280	19.90	−17.40	4	0.03	−0.621	0.130	2	...	...	...
Dwarf Spherical																		
FOR	237.3	−65.7	dSph	0.1	4	1.100	6	−0.190	25.60	−12.00	6	0.10	−0.320	0.067	3	...	...	...
SCL	147.2	−85.2	dSph	0.1	4	0.800	7	−0.590	25.10	−10.50	6	0.05	...	0.041	3	...	...	...
CAR	260.2	−22.3	dSph	0.1	4	0.790	7	−0.700	26.30	−8.80	6	0.06	...	0.052	3	...	...	...
DRA	86.4	34.7	dSph	0.1	4	1.050	7	−0.820	26.50	−7.90	6	0.07	...	0.015	3	...	...	...
UMI	105.0	44.8	dSph	0.1	4	1.000	7	−0.700	27.20	−7.90	6	0.03	...	0.008	3	...	...	...

TABLE 1—*Continued*

Name (1)	l (2)	b (3)	Type (4)	Distance (Mpc) (5)	Source (6)	log σ_0 (km s^{-1}) (7)	Source (8)	log r_e (kpc) (9)	SB_e (mag arcsec^{-2}) (10)	M_T (11)	Source (12)	A_B (13)	log $(v/\sigma_0)^*$ (14)	Mg_2 (15)	Source (16)	$(B-V)_0$ (17)	Source (18)	a_4 (19)
								Bulges										
N16.....	111.6	−34.2	LX	67.6	5	2.260	9	0.366	19.59	−20.80	8	0.17	0.3	...	...	0.93	2	3.50
N474	136.8	−58.7	LAS0	51.0	5	2.233	9	0.356	20.09	−20.25	8	0.06	0.3	...	...	0.82	2	3.50
N936	168.6	−55.3	LBT	30.2	5	2.286	9	0.555	20.41	−20.92	8	0.05	0.3	0.297	4	0.95	2	3.50
N1175	147.7	−14.1	LAR	113.7	5	2.301	8	0.640	20.10	−21.75	7	0.56	−0.130	...	...	0.85	2	3.50
N1553	265.6	−43.7	LAR0	21.1	5	2.230	10	0.348	19.24	−21.06	7	0.00	−0.036	...	...	0.87	2	3.50
N2549	159.7	34.2	LAR0	24.1	5	2.146	8	−0.030	18.80	−19.72	7	0.12	0.040	0.297	5	0.93	2	3.50
N2639	168.9	38.2	RSAR	65.4	5	2.255	11	0.872	22.02	−20.90	8	0.10	0.3	0.261	2	0.80	2	3.50
N2776	175.5	43.3	L	53.5	5	1.875	11	...	...	...	9	0.04	0.3	0.178	2	0.48	2	3.50
N2778	189.2	43.0	LA	39.6	6	2.274	9	0.054	20.69	−18.14	8	0.02	0.3	0.337	4	0.91	2	3.50
N2880	151.5	41.8	LB	32.9	5	2.158	9	0.387	20.60	−19.90	8	0.09	0.3	...	...	0.88	2	3.50
N2916	208.7	45.2	SAT3	71.9	7	2.134	11	...	...	...	9	0.07	0.3	0.255	2	0.59	2	3.50
N3098	206.8	52.1	L	25.4	5	2.021	8	...	...	...	9	0.10	0.3	0.235	5	0.86	2	3.50
N3300	228.5	56.1	LXR0	57.3	5	2.164	11	0.377	21.04	−19.41	8	0.07	0.3	0.278	2	...	...	3.50
N3115	247.8	36.8	L	8.7	5	2.342	1	0.189	19.75	−19.70	7	0.10	0.120	0.309	1	0.97	1	3.50
N4026	142.0	64.2	L	19.0	5	2.204	8	−0.270	18.20	−19.10	7	0.04	−0.050	0.270	5	0.90	2	3.50
N4036	133.0	54.3	L	30.2	5	2.290	9	0.267	20.21	−19.69	8	0.03	0.3	0.285	5	0.89	2	3.50
N4111	149.5	71.7	LAR	16.5	5	2.176	8	−0.480	17.90	−18.33	7	0.00	−0.070	0.264	5	0.88	2	3.50
N4169	197.4	81.1	L	76.5	5	2.346	9	0.687	20.76	−21.24	8	0.02	0.3	...	...	0.91	2	3.50
N4281	282.8	67.0	L	49.0	5	2.455	9	0.850	21.37	−21.44	8	0.00	0.3	0.314	4	0.94	2	3.50
N4350	270.2	77.8	LA	20.7	5	2.290	8	...	...	...	9	0.03	0.3	0.341	5	0.93	2	3.50
N4594	298.5	51.2	SAS1	17.5	5	2.342	8	0.910	21.00	−22.51	7	0.12	−0.050	0.330	4	0.84	2	3.50
N5308	111.3	54.9	L	43.6	5	2.350	8	...	...	...	9	0.01	0.3	0.295	4	0.90	2	3.50
N5380	74.3	72.7	LA	61.2	5	2.199	11	0.030	19.10	−19.61	8	0.00	0.3	0.327	2	0.93	2	3.50
N5422	103.5	59.3	L	39.2	5	2.258	11	...	...	...	9	0.00	0.3	0.323	2	...	...	3.50
N7332	87.4	−29.7	LP	29.7	5	2.130	8	0.010	18.30	−20.41	7	0.11	−0.110	0.263	5	0.87	2	3.50

NOTES.—

(Col. [1]) Galaxy name according to major catalogs.

(Cols. [2] and [3]) Galactic longitude (b) and Galactic latitude (l), according to de Vaucouleurs et al. (1976; hereafter RC2), Sulentic & Tifft (1974, hereafter RNGC), and as derived from the celestial coordinates given in Binggeli et al. (1985).

(Col. [4]) Type according to RC2 and Binggeli et al. (1985). Exceptions are: NGC 147, NGC 185, and NGC 205 were reclassified as dE (originally E in RC2); NGC 3641, NGC 4467, and VCC 351 were reclassified based on CCD-photometry by Prugniel (1989) (originally cE and cE candidates in RC2 and Binggeli et al.); and the type of NGC 2778 taken from Kent (1985).

(Col. [5]) Distances in Mpc ($H_0 = 50$ km s^{-1} Mpc^{-1}).

(Col. [6]) Sources for distances: 1 = group redshift from Faber et al. (1989) corrected to centroid of Local Group; 2 = individual redshift from Faber et al. (1989) corrected to centroid of Local Group; 3 = Sandage & Tammann (1981); 4 = Zinn (1985); 5 = individual redshift from Sandage & Tammann (1981) corrected to centroid of Local Group; 6 = individual redshift from Davies et al. (1983) corrected to centroid of Local Group; 7 = individual redshift from Bender (unpublished) corrected to centroid of Local Group.

(Col. [7]) Log σ_0, logarithm of central velocity dispersion (σ_0), in units of km s^{-1}.

(Col. [8]) Sources of values of σ_0: 1 = Davies et al. (1987); 2 = Tonry (1984); 3 = Bender et al. (1991); 4 = Bender & Nieto (1990); 5 = Bender, unpublished; 6 = Mateo et al. (1991); 7 = Freeman (1987); 8 = Seifert (1990); 9 = Whitmore et al. (1985); 10 = Kormendy & Illingworth (1982); 11 = Bender (unpublished).

(Col. [9]) Log r_e, logarithm of effective half-light radius, r_e, in kpc, for the whole galaxy (ellipticals) and for the bulge only (spirals and S0's). The value for r_e is derived from an $r^{1/4}$ fit to the growth curve, or from an $r^{1/4}$ fit to surface brightness profile as a function of $(a \times b)^{1/2}$. The value of r_e for dwarf spheroidals is derived from core and tidal radii via King models.

(Col. [10]) SB_e, mean surface brightness within effective radius in B-band for the whole galaxy (ellipticals) and only for the bulge (spirals and S0's), in B-mag arcsec^{-2}.

(Col. [11]) M_T, absolute magnitude in B-band for the whole galaxy (ellipticals) and only for the bulge (spirals and S0's).

(Col. [12]) Sources for r_e, SB_e, and M_T: 1 = Burstein et al. (1987); 2 = Burstein et al. (1987), corrected by unpublished CCD photometry; (3) = RC2 and Kent (1987); 4 = Prugniel (1989); 5 = Binggeli 1992, private communication, and own unpublished CCD photometry; 6 = Freeman (1987) and assuming $(B-V)_0 = 0.6$ mag; 7 = Seifert (1990); 8 = Kent (1985).

(Col. [13]) Galactic extinction, A_B from Burstein & Heiles (1984), and Burstein (unpublished).

(Col. [14]) The anisotropy parameter $(v/\sigma_0)^*$, expressed in logarithmic form, derived in accordance with Bender & Nieto (1990). Sources of data are Schechter & Gunn (1979); Kormendy & Illingworth (1982); Davies & Illingworth (1983); Davies et al. (1983); Tonry (1984); Paltoglou & Freeman (1987); Bender (1988a); Davies & Birkinshaw (1988); Franx et al. (1989); Bender & Nieto (1990); Bender et al. (1991); and Bender (unpublished).

(Col. [15]) The Mg_2 index, defined according to Burstein et al. (1984) and Faber et al. (1985).

(Col. [16]) Sources for Mg_2: 1 = Davies et al. (1987); 2 = Bender (unpublished; value for NGC 205 is at 100 pc from starlike nucleus); 3 = based on [Fe/H] (Aaronson & Mould 1985; Caldwell et al. 1992), calculated using the globular cluster calibration given by Burstein et al. (1984); 4 = Faber, Burstein et al. (unpublished); 5 = Paquet et al. (1992, 1993).

(Col. [17]) The $(B-V)_0$ color, corrected for Galactic extinction according to the value in col. (13).

(Col. [18]) Sources for $(B-V)_0$: 1 = Burstein et al. (1987); 2 = RC3 (computer disk copy as provided by H. C. Corwin).

(Col. [19]) The isophotal shape parameter a_4/a. Negative values indicate boxy isophotes, positive values disky isophotes. No entry indicates irregular isophote or no measurement; $a_4/a = 3.50$ is the default value for bulges. Data come from Bender et al. (1989) and Bender (unpublished).

the same system as used for normal ellipticals and bulges, we derived Mg_2 indices based on the globular cluster $Mg_2 - Z$ calibration of Burstein et al. (1984). The accuracy of this procedure is verified by two objects (NGC 147 and NGC 205) for which direct Mg_2 measures compare well with metallicity estimates from color-magnitude diagrams (e.g., Freedman 1992). The measured Mg_2 for NGC 205 refers to the stellar population 100 pc from the starlike nucleus of this galaxy.

3. Central Mg_2 measures for seven S0 bulges were taken from the data sample of Paquet, Bender, & Seifert (1992, 1993), and velocity dispersions for these objects were taken from the compilation of Whitmore, McElroy, & Tonry (1985) and from Seifert (1990). Mg_2 values for seven bulges in S0's and spirals were taken from the unpublished observations of Faber et al. Six of these bulges supplement the sample used in B^{2}F1.

4. $(B-V)_0$ colors, corrected for redshift and reddening, were taken mainly from the 7 Samurai data set, using the values listed in Burstein et al. (1987). These colors refer to an average of all color measurements within an aperture of 67″ diameter, or an aperture $\sim 25\times$ the size of the typical aperture used to measure Mg_2, but typically $\frac{1}{2}$ to $\frac{2}{3}$ the effective radius. The 7 Samurai did not obtain colors for dwarf ellipticals and bulges. For these, we used total corrected $(B-V)_0$ colors from the Third Reference Catalog of Bright Galaxies (de Vaucouleurs et al. 1991, hereafter RC3). The $(B-V)_0$ colors taken from the RC3 were constructed to predict the *total* color of a galaxy. The RC3 estimates of color gradients in normal ellipticals suggest that the total RC3 colors might yield $(B-V)_0$ colors that are too blue by 0.01–0.02 mag, relative to the 7 Samurai colors.

Additional spectra, primarily for dwarf ellipticals and bulges, were obtained by RB at the 2.2 and 3.5 m telescopes of the German-Spanish Astronomical Center, Calar Alto, Spain (see Table 1). The kinematic results from these observations have mostly been published elsewhere (Bender & Nieto 1990; Bender, Paquet, & Nieto 1991). Observational details, instrumental set-ups and standard reduction procedures can be found in these publications. Central velocity dispersions were tabulated in B^{2}F1. For this paper, Mg_2 indices were measured from the same spectra and transformed to the Faber/Burstein system (Burstein et al. 1984; Faber et al. 1985).

When needed, we use $H_0 = 50$ km s^{-1} Mpc throughout this paper (most of the quantities are distance-independent, however). A full discussion of the structural parameters for these galaxies is given in B^{2}F1.

3. THE Mg_2–σ RELATION FOR DHGs

3.1. *Bright Elliptical Galaxies*

Faber (1973) discovered that metal line-strengths (e.g., Mg_2) increase with luminosity (M_T) among elliptical galaxies and interpreted this rise as due to an increase in metallicity with increasing mass. Subsequently, Terlevich et al. (1981) found that the residuals from the Mg_2–M_T relation correlated with the residuals from the σ_0–M_T relation (the so-called δ–δ relation). Terlevich et al. also claimed that the ellipticities of the galaxies were correlated with these residuals. To investigate these findings in more detail was the main motivation for the 7 Samurai project (Faber et al. 1987).

As a result of the 7 Samurai study and the study of Djorgovski & Davis (1987), we now know that the luminosity of elliptical galaxies is not the optimum parameter to be compared with their Mg_2-values. Part of the original δ–δ effect can be removed by replacing M_T with a combination of M_T and surface brightness. A further contribution to the δ–δ effect came from distance errors, as revealed by the 7 Samurai survey. Finally, as is now well-known, the ellipticity connection also was spurious, due to small number statistics. Most of the original motivation for the 7 Samurai survey turned out, ironically, to be wrong!

All of the studies that have subsequently looked at Mg_2 with good data and large samples have shown that the relationship between Mg_2 and σ_0 is tight for bright ellipticals (Terlevich et al. 1981; Dressler 1984; Dressler et al. 1987; Burstein et al. 1988b). Similar conclusions have been reached with respect to $U-V$ and $V-K$ colors by Ellis (1992) and Bower, Lucey, & Ellis (1992).

In their analysis of the data for bright ellipticals in the 7 Samurai sample, Burstein et al. (1988b) found that the residuals of Mg_2 on σ_0 have a Gaussian core with a standard deviation of 0.016 mag in Mg_2, close to the expected observational error of 0.015 mag (§ 3.2). The relationship between Mg_2 and σ_0 for these 455 ellipticals is shown in Figure 2. The full line drawn is a least-squares fit to the data by Burstein et al. (1988b), $Mg_2 = 0.175 \log \sigma_0 - 0.11$; the dashed line is a fit to all data used in this paper (see below).

Burstein et al. (1988b) also showed that, in addition to this Gaussian core, a minority of ellipticals ($\leq 20\%$) form a tail in these residuals, in the sense that these galaxies have significantly weaker Mg_2 at a given σ_0 than the majority of the sample. The residual distribution is therefore skewed, with a tail to negative values. This effect is found with about equal frequency among both the field and the cluster sample of the 7 Samurai (cf. Dressler et al. 1987; Burstein, Faber, & Dressler 1990) and has been studied by Schweizer et al. (1990) and Gregg (1992). This scatter, while significant, is nonetheless a secondary effect in the Mg_2–σ_0 relationship. It will be further discussed in § 3.4.

A final point is that the distribution of Mg_2 residuals appears to broaden significantly at low values of σ_0 in Figure 2. More precisely, the total range of residuals appears unchanged, but the tight core of points around zero disappears at low σ_0. The formal rms spread in the residuals roughly doubles from high σ_0 to low σ_0. Increased observational errors for small galaxies may play a role but is not likely to be the whole story because many of these small galaxies were observed many times. Or, perhaps the scatter among low-luminosity systems has a different physical origin than that among bright galaxies (e.g., through a combination of age and metallicity effects; see Faber et al. 1992 for other thoughts on this matter).

A third possibility appeals to the GS continuum merger idea, in which each of these galaxies is built up by a succession of merger events. It logically follows that formation of the smaller systems would involve fewer mergers, in which case there might be a larger statistical scatter in the metallicity of the final galaxy, there being fewer "formation events" to average over. In any case, it is interesting that small ellipticals appear to be less homogeneous in some sense than large ones. This could equally well reflect a greater spread in relative ages as in relative metallicities.

3.2. *Other Types of DHGs*

The extension of the Mg_2–σ_0 relation to all DHGs studied in B^{2}F1 is shown in Figure 3. The meaning of the symbols is the same as in Figure 1. For visual clarity, the 7 Samurai bright

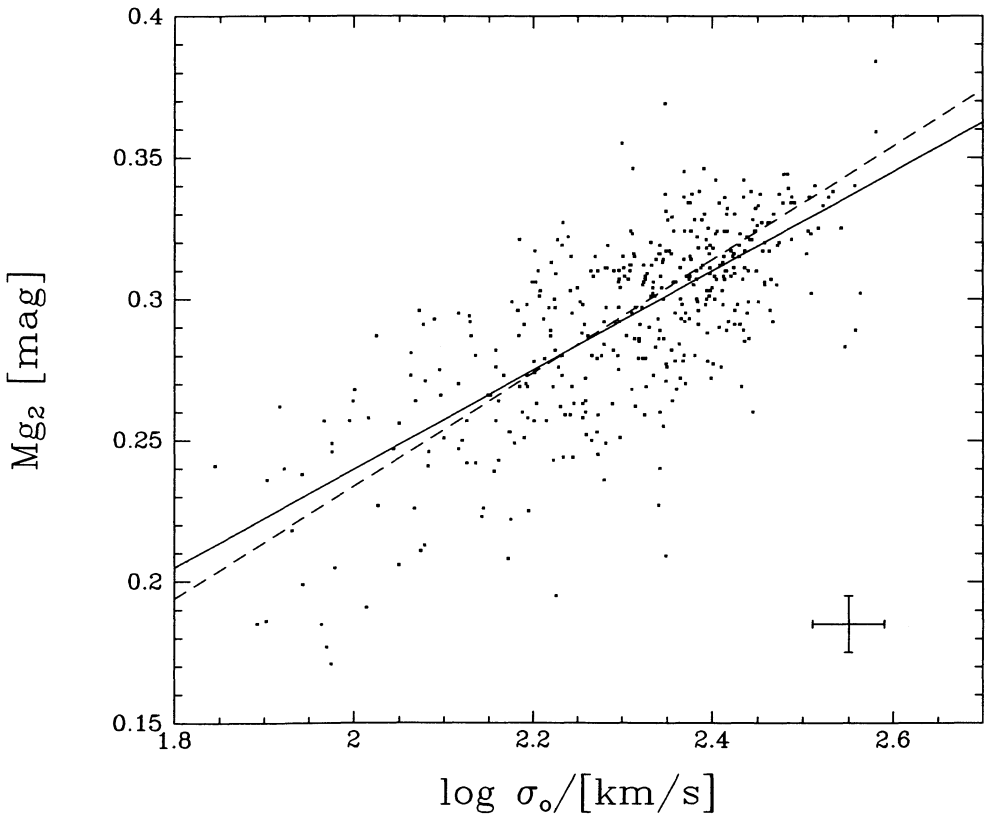

FIG. 2.—Nuclear Mg_2 absorption line index plotted against $\log \sigma_0$ (central velocity dispersion) for the 7 Samurai sample of elliptical galaxies (Faber et al. 1989). The full line drawn is the fit given by Burstein et al. (1988b), the dashed line is the relation adopted in this paper (see Fig. 3). Either relation is compatible with the 7 Samurai data. A typical error bar is shown.

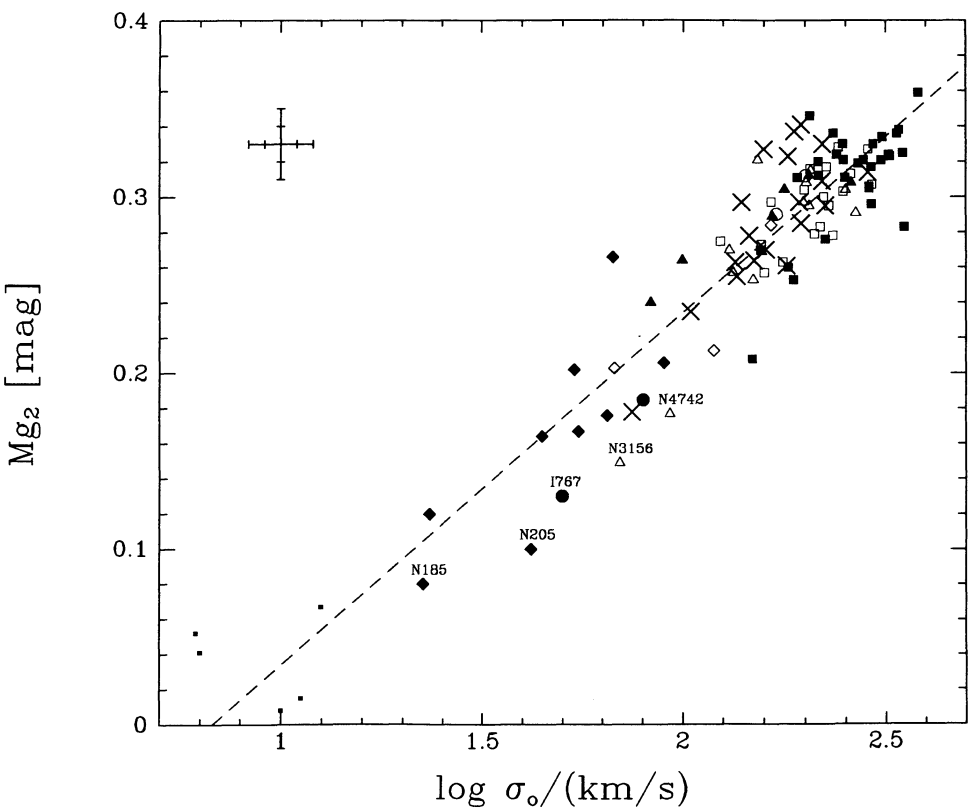

FIG. 3.—Nuclear Mg_2 index plotted against σ_0 for all types of DHGs (symbols coded as in Fig. 1). The dotted line represents the relation $Mg_2 = 0.20 \log \sigma_0 - 0.166$. Galaxies which show evidence for young or intermediate age stars are labeled. Representative error bars are shown in the upper left, the larger error bars refer to the objects with low values of σ_0, the smaller ones to luminous ellipticals and bulges. The Mg_2–$\log \sigma_0$ correlation is tight over many decades in galaxy size and all DHG types.

ellipticals are not replotted in this diagram. It is clear upon inspection that the Mg_2–σ_0 relation defined by bright ellipticals is continued for all DHGs, even down to the faintest dwarf spheroidals. A least-squares fit to the data in Figure 3 yields the relation $Mg_2 = 0.20 \log \sigma_0 - 0.166$. While this fit is formally different from that obtained from the bright ellipticals alone, as shown in Figure 2, the two relationships are quite similar over the limited range covered by bright ellipticals. We explicitly emphasize that in the Mg_2–σ_0 relation there is no evidence for a significant zero-point difference between dwarf ellipticals and luminous ellipticals, contrary to what is observed in the relation between color (metallicity) and *luminosity* (Aaronson & Mould 1985). As surface brightness is the principal difference between dwarf ellipticals and bulges/luminous ellipticals of similar mass (cf. Fig. 1), it is likely that lower surface brightnesses of dwarf ellipticals produces the offset from luminous ellipticals in the color-luminosity diagram.

The relationship of scatter in the Mg_2–σ_0 relation to the known physical properties of DHGs can be examined in several ways. Of prime importance is the fact that residuals from the mean Mg_2–σ_0 relation do not appear to be correlated with positions of DHGs *within* the fundamental plane (cf. position of the extreme compact M32 relative to dwarf spheroidals in Fig. 3). Scatter in the Mg_2–σ_0 relation is also not correlated in a significant way with deviations of the objects *perpendicular* to the fundamental plane. This emphasizes that, despite a possibly large variety of formation histories, the stellar populations of dynamically hot galaxies virtually change in lockstep with velocity dispersion (i.e., with their kinematic "temperature").

Following the methodology established in B^2F1, in Figure 4 we compare residuals about the Mg_2–σ_0 relation to the degree of anisotropy as measured by $(v/\sigma_0)^*$. From Figure 4, it is clear that the scatter in Mg_2–σ_0 depends neither on the degree of anisotropy nor on the type of DHG considered. While some intrinsic scatter exists at all luminosities (a point raised earlier and further discussed below), the overall impression is that there is an astonishing agreement in slope, zero point, and scatter in the Mg_2–σ_0 relation for all DHGs. This tight relationship is all the more remarkable as it includes galaxies from both sequences within the fundamental plane—the GS continuum and the dwarf continuum—that were defined in B^2F1.

We have also checked whether Mg_2 residuals correlate with the isophotal shape parameter a_4/a (Fig. 5). This is of interest because isophotal shapes are known to correlate with radio and X-ray properties of ellipticals (Bender et al. 1989) as well as kinematic properties (Bender 1988a, 1990). Although a_4/a measurements are only available for normal ellipticals, we can infer at least for this group of galaxies that no significant correlation between the residuals and a_4/a exists, i.e., boxy and disky ellipticals basically follow the same Mg_2–σ_0 relation (see Fig. 5).

Finally, we note that the 7 Samurai study showed that the scatter of the Mg_2–σ_0 is comparable for both field and cluster galaxies (Dressler et al. 1987; Burstein et al. 1990). This suggests that the cause of this scatter is not strongly related to environment.

From the tightness of the Mg_2–σ_0 relation, powerful constraints on models of galaxy formation for DHGs can be derived. To do this, we need to estimate the intrinsic dispersion

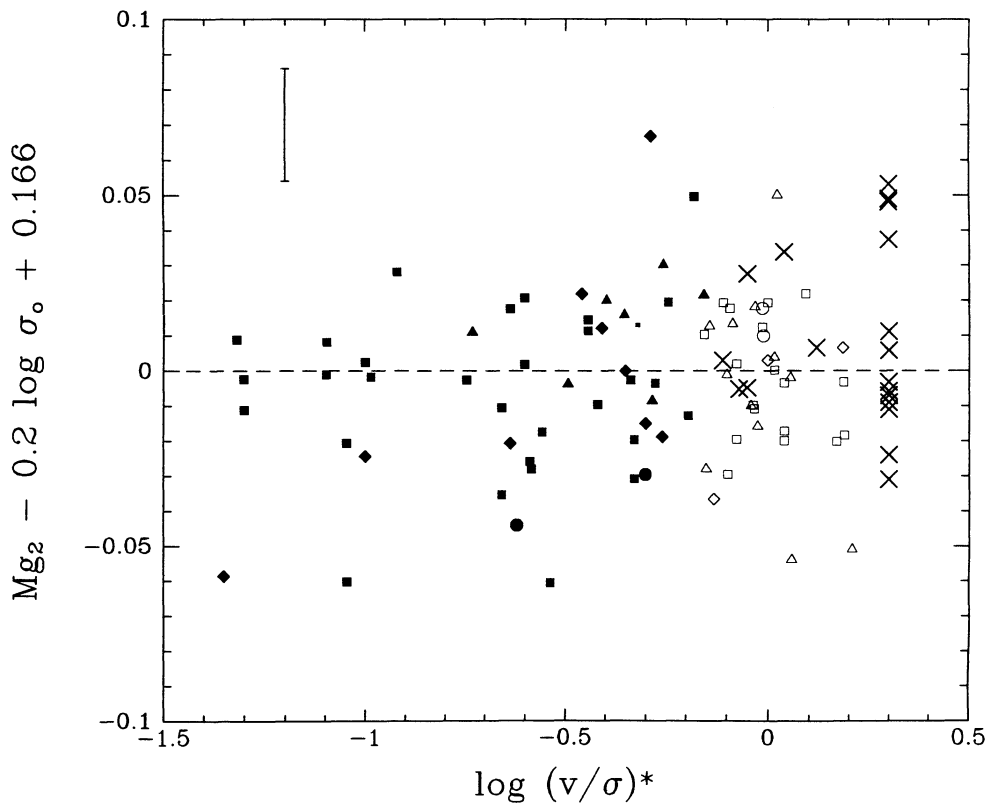

FIG. 4.—Residuals of the Mg_2–log σ_0 relation (Fig. 3) plotted against log $(v/\sigma)^*$ (velocity dispersion anisotropy; symbols coded as in Fig. 1). If $(v/\sigma)^* > 0.7$ [log $(v/\sigma)^* > -0.15$], the galaxy is assumed to be rotationally flattened; otherwise the galaxy is assumed anisotropic. Bulges (*crosses*) for which no $(v/\sigma)^*$ value is available have been plotted at log $(v/\sigma)^* = 0.3$. No significant trend is seen.

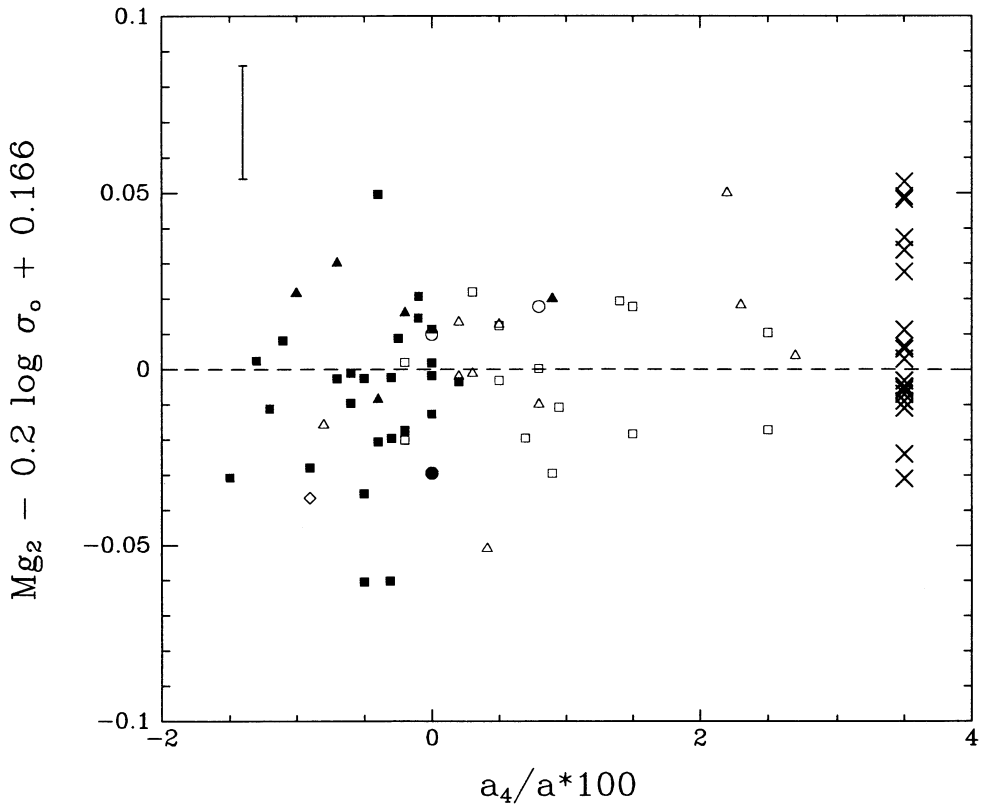

FIG. 5.—Residuals of the Mg_2–log σ_0 relation (Fig. 3) plotted against the isophotal shape parameter $a_4/a \times 100$. Symbols coded as in Fig. 1. Negative values of a_4/a indicate boxy isophotes, positive values of a_4/a represent disky isophotes. Bulges have been plotted at $a_4/a \times 100 = 3.5$. Again, no significant trend is seen.

of Mg_2 at a given velocity dispersion. The observational rms error in σ_0 is $\approx 10\%$, or $\Delta \log \sigma_0 \approx 0.04$ (somewhat smaller for luminous E's and somewhat larger for the low-luminosity objects). The measurement error in Mg_2 varies between 0.01 mag for giant E's and 0.02 mag for dwarf E's, i.e., ≈ 0.015 mag. If we remove these contributions in quadrature from the observed rms-scatter in Figure 3 ($\Delta Mg_{2,obs} \approx 0.025$ mag), we obtain for the intrinsic scatter an average of $\Delta Mg_{2,intr.} \approx 0.018$ mag over all systems. As noted before, dwarfs tend to have greater intrinsic scatter than bright ellipticals.

This scatter can be translated into age or metallicity variations by making use of population synthesis models. Considering the models of various authors (Mould 1978; Terlevich et al. 1981; O'Connell 1986; Peletier 1990; Charlot & Bruzual 1991; Faber et al. 1992), we derive the following approximate relation:

$$\log Mg_2 = 0.41 \log (Z/Z_\odot) + 0.41 \log (t/\mathrm{Gyr}) - 1.00 , \quad (1)$$

where Z denotes metallicity, t denotes age, and the uncertainty in the coefficients is about $\pm 20\%$ (most weight was given to the most recent models by Faber et al. 1992). This relation is relatively reliable for $-0.5 < \log (Z/Z_\odot) < 0.3$ and 5 Gyr $< t <$ 15 Gyr but also gives plausible results when applied to lower metallicity and/or younger populations (e.g., it gives a mean age lower than 1 Gyr for the young stars in the nucleus of NGC 205, consistent with other estimates Burstein et al. 1988a).[1]

Based on equation (1) the following conclusion can be derived:

a. Age spread.—If we attribute the intrinsic dispersion of 0.018 mag in Mg_2 *solely* to dispersion in age, two conclusions follow. First, the rms spread in age at fixed σ_0 is only about 15% averaged over the brighter systems and potentially much bigger for faint systems (up to 50% for the dwarf spheroidals). Second, in only a rather small fraction of bright DHGs ($\sigma_0 >$ 150 km s^{-1}) can the bulk of the stars be significantly younger than 5 Gyr, otherwise these objects would have an implausibly high metallicity. This is consistent also with the recent analysis by Schweizer & Seitzer (1993).

b. Metallicity spread.—Turning argument (a) around and assuming that the Mg_2 dispersion is due to metallicity *alone* implies that the metallicity spread at a given velocity dispersion also has to be rather small. Similar to case (a), we derive that the rms dispersion in metallicity Z is about 15% for the bright systems, and again significantly larger for the faintest ones. Once more, it should be kept in mind that this refers to

[1] It should be kept in mind that Mg_2 is a good indicator only for light element abundances. The very good correlation between Mg_2 and σ_0 does not necessarily imply a similarly good correlation between iron-peak elements and σ_0. Indeed, recent results (Peletier 1990; Faber et al 1992) indicate that, on average, the iron-peak elements are at most only slightly enhanced even when the abundance of light elements like Mg are strongly enhanced. The above models assume a solar ratio in Fe/Mg and thus are likely to overestimate somewhat the average Z in strong-Mg_2 galaxies.

light elements only and may be different (probably smaller) for iron peak elements.

c. Spread in σ_0.—The intrinsic dispersion in measured σ_0 as a function of the stellar population parameters likewise cannot be large. A basic lower limit to the expected dispersion in σ_0 is set by the anisotropy of the stellar velocity dispersions, which causes the line-of-sight dispersion to vary even when the total kinetic energy does not. The maximum total modulation (expressed relatively) is approximately 0.5× (ellipticity) for systems with constant anisotropy (Binney & Tremaine 1987), but the effect is reduced by about a factor of 2 in practice since few systems appear to be purely anisotropic. There is a further factor of 2 reduction since actual residuals are taken relative to mean inclination, not the extrema. The net result for an average set of galaxies with ellipticity $=0.3$ is only 0.02 in the logarithm of the mean projected velocity dispersion, and hence less than 0.04 mag in Mg_2. However, there is still the uncertainty of how closely the mean projected velocity dispersion is related to the observed *central* velocity dispersion σ_0, i.e., to the quantity which we actually compare with Mg_2. Furthermore, different shapes of the objects (e.g., prolate vs. oblate) may in principle add a further small amount of scatter.[2] These considerations suggest that variations in anisotropy and shape could contribute somewhat to the observed scatter in Mg_2 but are unlikely to account for its full amplitude.

There are other factors to be considered, stemming from the fact that we do not yet have a physical mechanism for why σ_0 correlates so well with stellar population parameters. It may be that σ_0 itself is the important variable, in which case there is no problem. But σ_0 may simply stand for something else, such as potential depth (i.e., escape velocity), whose relation to σ_0 might be close but not perfect, resulting in further scatter. Moreover, our measures of σ_0 are central values, whereas it might be physically more accurate to use a global σ_0 averaged over the whole galaxy. In either case, we must require that variations from galaxy to galaxy in the relevant kinematic and structural trends are small. These points are addressed again in § 4.

3.3. Mg_2 *versus* $(B-V)_0$ *for DHGs*

To this point we have been considering the relation between two parameters, Mg_2 and σ_0, that are derived from the same central spectra of galaxies, often the central 2″–3″. Our measure of stellar population can be considerably broadened to include a much larger fraction of a galaxy, however, if we substitute global $(B-V)_0$ for central Mg_2. Burstein et al. (1988b) showed that central Mg_2 indices, typically measured with a 2″ aperture, are essentially one-to-one correlated with $(B-V)_0$ colors averaged within a 67″ aperture. The relationship found there, $(B-V)_0 = 1.12Mg_2 + 0.615$ for 276 bright ellipticals with accurate reddenings, yields a scatter that is well-fitted by a Gaussian with a standard deviation of 0.023 mag, consistent with known observational errors.

The analogous relationship for all DHGs in Table 1 with measured colors and line strengths is shown in Figure 6. The line drawn in this figure is not fitted to these data, but is the relationship cited above for the 7 Samurai ellipticals. As before, the residuals from this correlation are plotted versus anisotropy index $\log (v/\sigma_0)^*$ in Figure 7 (the two bluest disk galaxies, NGC 2776 and NGC 2916 are not plotted here). There is a slight trend in Figure 7 in the sense that more anisotropic galaxies might be a little redder for their values of Mg_2 than isotropic galaxies. However, this interpretation depends critically on the inclusion of S0 bulges (*crosses*), for which some contamination of $(B-V)_0$ by disk light is occurring (Gregg 1989). Indeed, of the two bluest disk galaxies, one (NGC 2916) is the latest-type spiral in our sample (the other, NGC 2776, is an S0). Overall, except for the disk galaxies with the bluest global colors, the scatter in Figure 7 is consistent with observational errors with no significant trend. Furthermore, no difference is seen between the 67″ aperture (7 Samurai) colors and the total galaxy colors (RC3). This is probably true because the total color change beyond 34″ radius for most galaxies is fairly small.

As previously noted by Burstein et al. (1988b), the tight Mg_2–$(B-V)_0$ relationship requires that the stellar populations in the centers of elliptical galaxies be strongly coupled to the average stellar population throughout the bulk of the systems. The fact that essentially all DHGs effectively follow the same Mg_2–$(B-V)_0$ relation further emphasizes the degree of homogeneity among these stellar populations. Exceptions to this rule are objects like NGC 205, where centralized ongoing star formation causes a strong *positive* gradient in Mg_2 or $(B-V)_0$ (while all of the other objects where radial Mg_2 profiles are available show zero or negative gradients). The bright, nearly stellar nucleus of NGC 205 is known to have an A-type spectrum (Hodge 1989) and appears to be distinct from the rest of the low surface brightness core of this galaxy. The Mg_2 value given for NGC 205 refers to a region 20″ from the nucleus, within 100 pc of the core. Even at these radii, ongoing star formation is known to exist in NGC 205 (Hodge 1989). Likewise, the $(B-V)_0$ color will also be affected. Thus we a priori grant that any galaxy with ongoing star formation will not necessarily fit this relationship.

If the results of this section are now combined with those of the previous two, we infer that the strong correlation with central velocity dispersion must extend beyond the stars in the nuclei of non–star-forming DHGs to include the bulk of stars throughout the systems. To verify this explicitly, we show in Figure 8 the correlation between global $(B-V)_0$ and σ_0. As expected, the relation is tight. A further plot analogous to Figures 4 and 7 (not shown) confirms that the residuals from this relation show no correlation with the degree of anisotropy of the galaxy, as would be expected from combining Figures 4 and 7.

The fact that the central and bulk stellar populations are strongly correlated places rather strong constraints on the kinds of population gradients that can exist *within* galaxies. Discussion of these gradients is reserved for Paper III. For the present, it is sufficient to note that, when one refers to the Mg_2–σ_0 relation, one is evidently referring to the relationship of the stellar population of a galaxy *as a whole* to its central velocity dispersion.

3.4. *Is Age or Metallicity the Origin of the Intrinsic Dispersion in the* Mg_2–σ_0 *Relation?*

Our failure to find any relationship between intrinsic Mg_2 scatter and other structural parameters supports similar null results of Faber et al. (1987) and Burstein et al. (1990) for bright

[2] However, this effect is unlikely to be strong, because: (a) luminous ellipticals seem to be only slightly triaxial (near oblate) shapes (e.g., de Zeeuw & Franx 1991) and therefore should not be very different in shape from bulges; and (b) dwarf ellipticals appear to have a similar ellipticity distribution as luminous ellipticals, which in turn points to an intrinsic shape distribution similar to that of ellipticals (van den Bergh 1986).

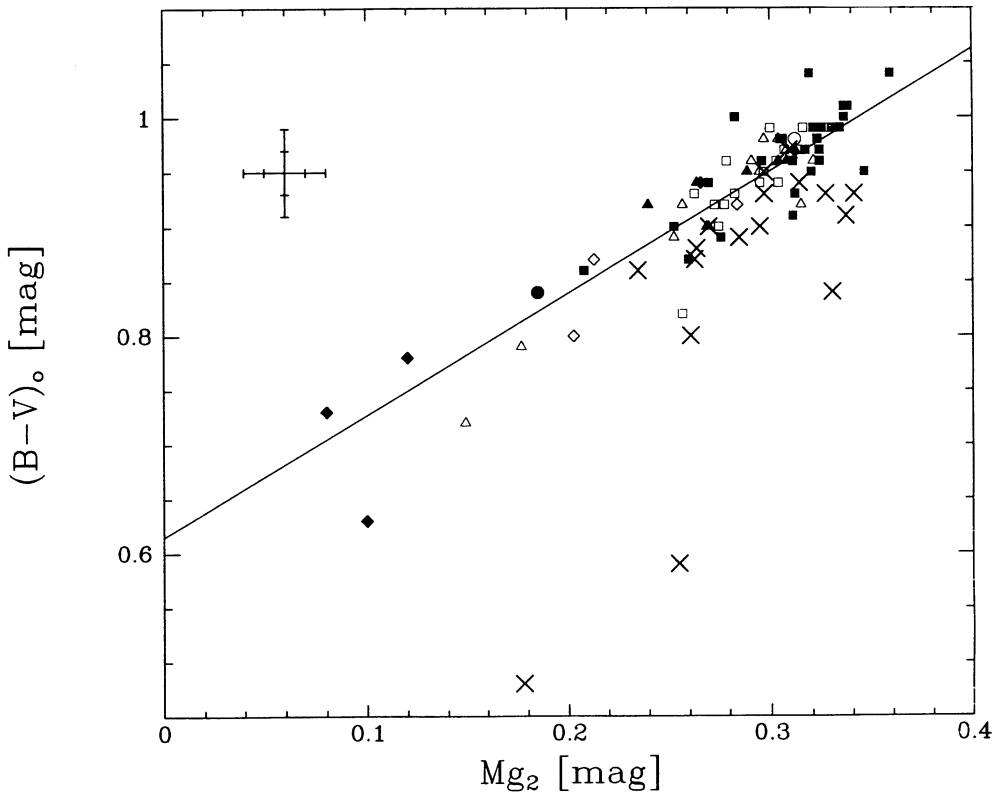

FIG. 6.—*Global* $(B-V)_0$ color index plotted against *nuclear* Mg_2. The line drawn here represents the relation $(B-V)_0 = 1.12Mg_2 + 0.615$ derived by Burstein et al. (1988*b*) for the 7 Samurai sample. Symbols are as in Fig. 1. Typical error bars are shown in the upper left. The smaller error bar on the Mg_2 axis refers ro bright E's and bulges, the bigger one refers to low-luminosity objects. The smaller error bar on the $(B-V)_0$ axis refers to measurements by the 7 Samurai, the bigger one to values from the RC3 (de Vaucouleurs et al. 1991). See Table 1 for source of data. The colors for disk galaxies are somewhat bluer than those of ellipticals at a fixed Mg_2, probably owing to the inclusion of a disk that is bluer than the bulge in the global color.

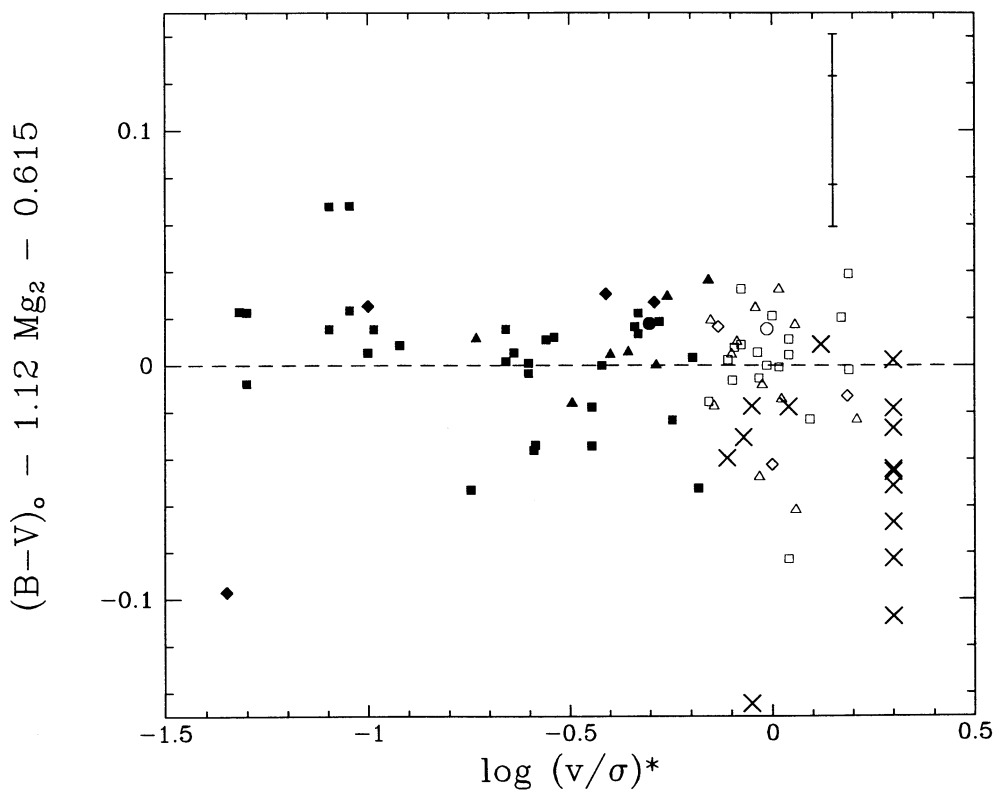

FIG. 7.—Residuals of the $(B-V)_0$–Mg_2 relation plotted against log $(v/\sigma)^*$ (velocity dispersion anisotropy; symbols coded as in Fig. 1. The slight apparent trend of residuals with anisotropy is mostly due to the bluer colors for a few disk galaxies. As discussed in the text, these blue global colors are more likely due to a blue disk rather than a blue bulge. Typical error bars are shown in the upper right (large error bar for low-luminosity objects, small error bar for ellipticals).

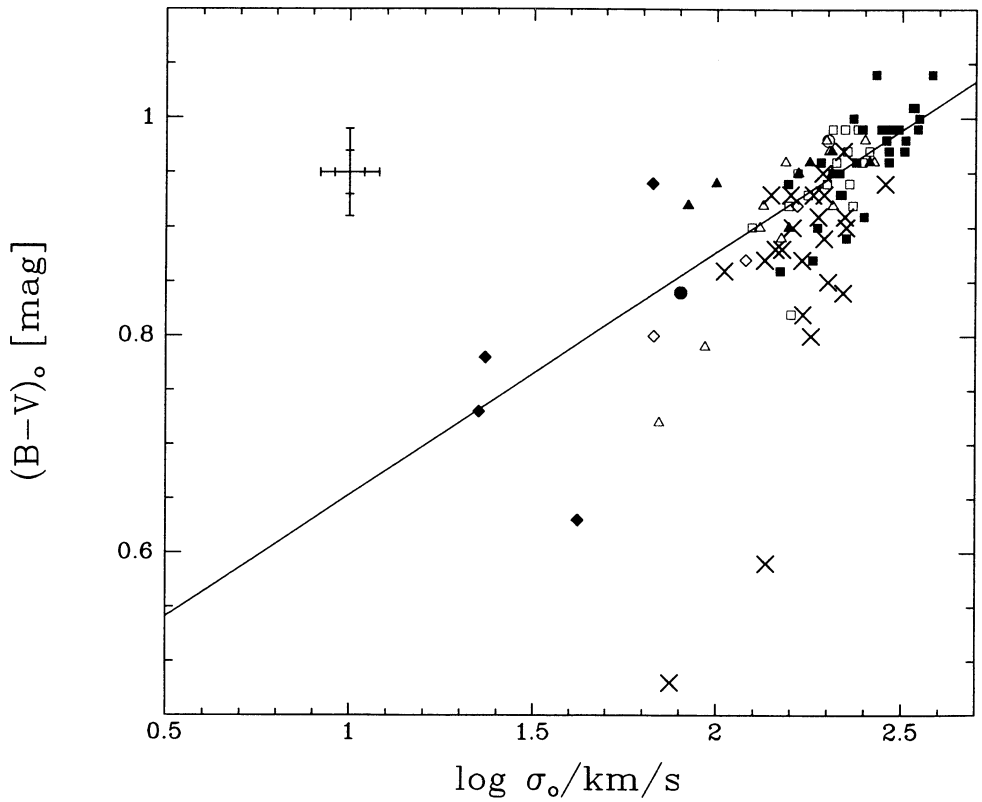

FIG. 8.—Global $(B-V)_0$ color index plotted against log σ_0. Symbols are the same as in Fig. 1. The line drawn through these data is not fitted per se, but results from combining the relations of Fig. 3 and Fig. 6: $(B-V)_0 = 0.224 \log \sigma_0 + 0.429$. Typical error bars are again shown in the upper left (for explanations see Figs. 3 and 6). Of the two bluest disk galaxies in this diagram, one (NGC 2916) is the latest-type spiral in our sample and the other (NGC 2776) is an S0.

ellipticals. However, it was shown by Schweizer et al. (1990) that, for at least some galaxies, Mg_2-weakness correlates positively with degree of morphological peculiarity, as quantified by the fine-structure parameter Σ defined in that paper.

As noted in § 1, Schweizer et al. left open the possibility that both age and metallicity variations weaken Mg_2 but gave preference in at least some cases to young age, given the more natural connection that would be expected with morphological peculiarities. Gregg (1992) confirmed the analysis of Burstein et al. and showed that the few galaxies in the Schweizer et al. sample with very weak Mg_2 probably have systematically bright magnitudes, presumably due to young stars. In the present sample, known star-forming galaxies such as NGC 3156, NGC 185, NGC 205, and NGC 4742 (Hodge 1989; Aaronson & Mould 1985; Gregg 1989; Burstein et al. 1988a) further support age differences. However, a counter-example is provided by NGC 5018, a giant elliptical nearly as weak-lined as NGC 3156 but without the obvious far-UV enhancement expected for a young stellar population (Bertola, Burstein, & Buson 1993). One is thus still left with the possibility that both age *and* metallicity differences contribute to the "weak-Mg_2" phenomenon.

Schweizer et al. stressed the natural connection expected between weak Mg_2 and morphological peculiarities in the gas-rich merger picture. In this scenario, recent mergers triggered both the morphological peculiarities and the starbursts that dilute Mg_2. This interpretation is consistent with the gas/stellar continuum picture for normal bright DHGs offered by B^2F1: in this picture, Mg_2-weak galaxies are simply those that suffered the most recent mergings or accretion events.

Ellipticals with kinematically peculiar cores are yet another class of objects which are believed to have experienced a major merging event (Bender 1988b, 1990; Franx & Illingworth 1988; Jedrzejewski & Schechter 1988; Schweizer 1990; Hernquist & Barnes 1991). It is therefore of interest to examine them for weak Mg_2 and the blue $(B-V)_0$ colors as well.

Figure 9 plots Mg_2 and $(B-V)_0$ versus σ_0 for the 7 Samurai sample of ellipticals. Ellipticals with kinematically peculiar cores are highlighted as solid squares in the left-hand panels (Figs. 9*a* and 9*b*). Galaxies from Schweizer et al. that have large values of the fine-structure parameter Σ are highlighted as solid squares in Figures 9*c* and 9*d*. The Schweizer et al. objects show strong bluing and Mg_2 dilution, as is already known. The peculiar-core galaxies may show a bluing trend similar to that of the high-Σ galaxies, but it does not appear to be as marked. Perhaps interactions producing peculiar core kinematics need not contain as much gas as those producing high-Σ galaxies. More likely, peculiar cores may have such long dynamical lifetimes that their accompanying starbursts have long since died away (the latter is supported by the observed radial Mg_2 profiles of ellipticals with peculiar cores, Bender & Surma 1992).

Finally, to place this section into perspective, we emphasize again that the intrinsic scatter in the Mg_2–σ_0 and the $(B-V)_0$–σ_0 relations are small in absolute terms. In all but the most blatantly star-forming galaxies such as NGC 205, such

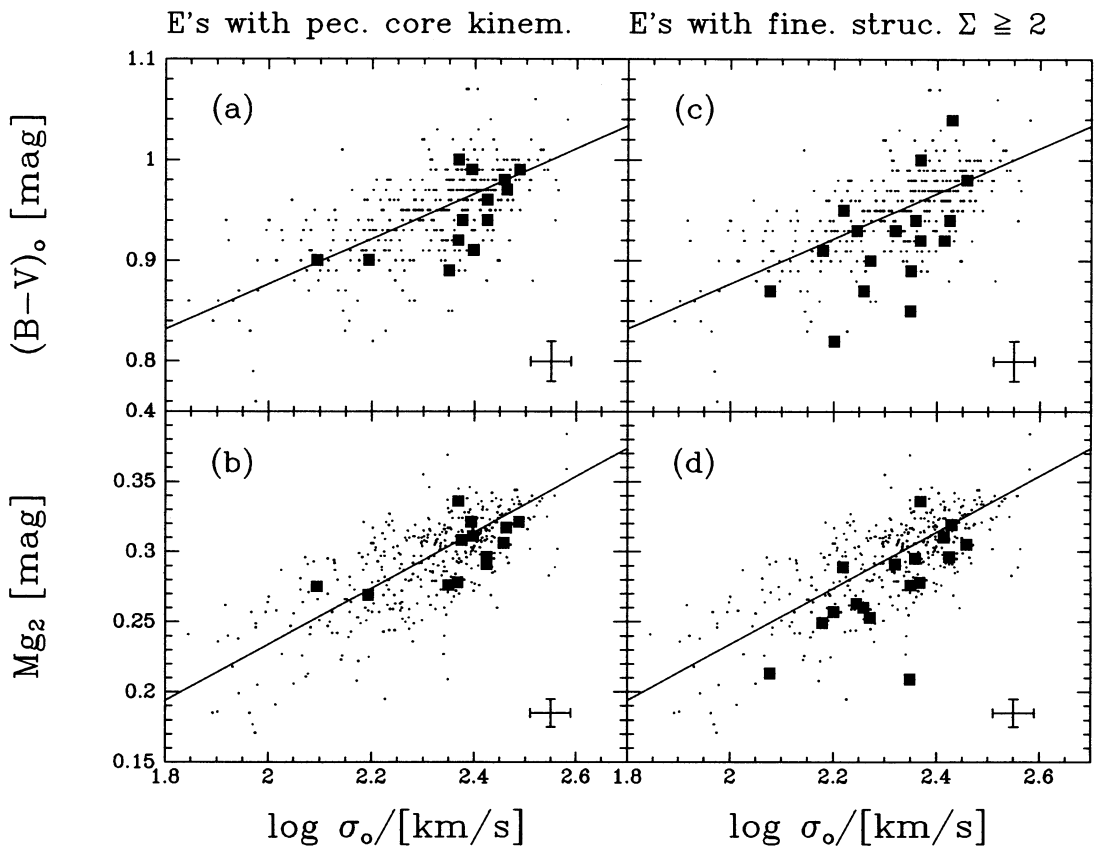

FIG. 9.—Nuclear Mg_2 and global $(B-V)_0$ plotted against log σ_0 for all 7 Samurai elliptical galaxies (*small symbols*). The data are plotted in (*a*) and (*c*), and in (*b*) and (*d*). Galaxies with known peculiar core kinematics are highlighted as big symbols in the left-hand panels (*a*) and (*b*) (see Bender 1990 for galaxy identification). Elliptical galaxies with fine-structure parameter $\Sigma \geq 2.0$ are identified as big symbols in (*c*) and (*d*) (see Schweizer et al. 1991 for galaxy identification). Lines drawn in (*a*) and (*c*) and in (*b*) and (*d*) come from Fig. 3 and Fig. 8, respectively. The result of Schweizer et al. is apparent in (*c*) and (*d*); high-Σ galaxies are bluer at a given σ_0 than are the overall sample. Galaxies with peculiar core kinematics (*a*) and (*b*) also tend to be bluer than most ellipticals.

scatter can be detected only with very accurate data. The basic, tight Mg_2–σ_0 relation is more important than the scatter about it.

4. ON THE ORIGIN OF Mg_2–σ_0

Neither of the parameters in Mg_2–σ_0 is easy to interpret physically. It has been customary to equate Mg_2 with mean Z or the mean temperature of the giant branch (e.g., Burstein 1985). However, more detailed models indicate that nonsolar abundance ratios are significant and that the strong Mg_2 enhancement seen in some giant ellipticals is in large part related to an overabundance of Mg per se (Faber et al. 1992). These models also show that age and abundance have very similar effects on both color and Mg_2, so that without more information, we cannot disentangle the two (see also § 3.2). In interpreting the tight Mg_2–σ_0 relation we can conclude only that the scatter in age at a given composition must be small, and vice versa. And exactly what is meant by "composition" is not yet clear.

The physical interpretation of σ_0 is likewise not straightforward. A priori, one can think of a number of plausible physical mechanisms that could relate σ_0 to metallicity and/or age. For example, σ_0 may modulate star formation through the cloud-cloud collision velocity, which in turn may control the IMF, and thus the absolute and relative yields of various elements (Faber et al. 1992). The same cloud-collision velocity could modulate the rate of star formation via the strength of shocks (Silk 1992), and hence the apparent age of the stellar population. Age could then be correlated with mean metallicity if cloud-collision velocity were correlated with the mass of the galaxy. Unfortunately, our current level of ignorance of these physical processes permits a wide range of speculation.

An alternative approach is to assume that σ_0 is an indicator of the mean potential depth of a galaxy. The connection to metallicity then involves the relative amount of gas loss, and hence the effective yield. This is indeed the classic way of explaining the higher metallicities of giant ellipticals (e.g., van den Bergh 1972; Larson 1974; Dekel & Silk 1986; Vader 1987; Yoshii & Arimoto 1987), by assuming that their deeper potential wells retain more heavy elements. Franx & Illingworth (1990) have carried this idea one step farther and assumed that the *local* metallicity within luminous ellipticals is completely determined by the *local* escape velocity. They achieved a fairly satisfactory fit to the mean color index profile of giant E's, but the fact that certain galaxies were found to deviate considerably from the mean relation indicates that this cannot be the whole story.

Indeed, within the picture of hierarchical formation of galaxies (which is supported by our considerations in B^2F1) it is difficult to conceive how an object that undergoes several merging or accretion events can build up or maintain a close link between *local* escape velocity and *local* metallicity (globally this may still be possible). Furthermore, the observations (e.g., Schweizer 1990; Kormendy & Sanders 1992) and

simulations (Hernquist & Barnes 1991) of merging galaxies show that enriched gas is efficiently transported to the center of the potential well during a merger event. This may result both in the formation of a kinematically decoupled core component and in the creation of a central metallicity gradient (Bender 1992; Bender & Surma 1992). Therefore, within the hierarchical merger picture, metallicity gradients are more likely to be built up by inflow of enriched material rather than by radially varying outflow.[3] Of course, inflow also has the virtue to explain the high central metallicities in giant ellipticals in a natural way, without having to invoke very high yields.

These latter considerations suggest a heuristic picture in which *one* parameter that determines *local* metallicity within DHGs is related to *local* stellar density (see also Edmunds 1992). The reasons are the following:

1. Local density is a crude measure of the amount of density enhancement over the mean initial background density and therefore is a measure for the amount of inflow or dissipation having taken place.

2. Local stellar density within a hierarchically formed object reflects, within limits, the stellar density of and within the subunits that merged (denser regions in the progenitors end up in the denser regions of the merger due to dynamical friction and approximate conservation of phase space density).

3. If, according to reason 2, the present local stellar density is related to the density in earlier sub-units and, ultimately, to the gas density out of which the stars formed, then the present local density still reflects the efficiency of density-dependent ISM processes such as cooling rate and star-formation rate.

Combining these arguments led us to consider a hybrid model to describe the stellar populations of DHGs. This hybrid model combines both global and local viewpoints by assuming that the stellar population of a DHG (represented schematically by the letter P) is determined by a combination of *total* mass $\boldsymbol{M}$ and local stellar volume density ρ (we neglect dark matter for the moment). Specifically,

$$P = f(\boldsymbol{M}^{\alpha}\rho^{\beta}) . \tag{2}$$

This is a relation between *local* P on the one hand and *local* density and *global* mass on the other hand.

The global Mg_2–σ_0 relation can be used to constrain the values of α and β in equation 2. Provided galaxies have similar radial distributions of density, one can take the global average of both sides of equation 2 to obtain $\langle P\rangle = f(\boldsymbol{M}^{\alpha}\langle\rho\rangle^{\beta})$. Then using

$$\boldsymbol{M} = c_2\,\sigma_0^2\,r_e \tag{3}$$

and

$$\langle\rho\rangle = c_3\,\boldsymbol{M}/r_e^3 \tag{4}$$

(where the constants c_2 and c_3 are functions of the detailed structure of a galaxy), we obtain

$$\sigma_0^6 = (c_3\,c_2^3)^{-1}\boldsymbol{M}^2\langle\rho\rangle . \tag{5}$$

Reproducing the observed tight global dependence of Mg_2 on velocity dispersion thus requires the ratio $\alpha/\beta = 2$. If we insert the last equation into the observed Mg_2–σ_0 relation we obtain:

$$Mg_2 = 0.033 \log (\boldsymbol{M}^2\langle\rho\rangle) + \text{constant} , \tag{6}$$

where the constant is a function of c_2 and c_3. Similarly, using the observed correlation of Mg_2 and $(B-V)_0$, we find that

$$(B-V)_0 = 0.037 \log (\boldsymbol{M}^2\langle\rho\rangle) + \text{constant} . \tag{7}$$

The existence of constants in these relationships (related to the details of galaxy structure) suggests that the intrinsic scatter might be related in some way to variations in the constants. A further, more speculative extrapolation of this formulation might include galaxies with dark matter. For such galaxies, $\boldsymbol{M}$ in our picture should refer to the total mass of the galaxy including dark matter, while ρ should refer only to the average baryonic density, as star formation and cooling processes are basically determined by the baryonic density only.

This reformulation of the Mg_2–σ_0 relation in terms of $\boldsymbol{M}$ and ρ serves as the lead-in to the third paper in this series, where we will investigate whether the $\boldsymbol{M}^2\rho$ formulation is able to predict the correct P gradients within DHGs. Furthermore, we will test the three hypotheses (i.e., metallicity determined by σ_0, v_{esc}, or $\boldsymbol{M}^2\rho$) against each other.

5. CONCLUSIONS

In this paper we have analysed the relations between global stellar populations and structural properties of dynamically hot galaxies (DHGs—giant ellipticals, low-luminosity ellipticals, compact ellipticals, diffuse dwarf ellipticals, dwarf spheroidals, and bulges). We find that:

1. All DHGs follow a single relationship between global stellar population (as represented by Mg_2 index or $B-V$ color) and central velocity dispersion σ_0. The Mg_2–σ_0 relation is significantly tighter than the relation between the Mg_2 index and *absolute luminosity*, especially for $-15 > M_T > -19$; the residuals from the latter relation appear to be correlated with surface brightness.

2. The relation between central Mg_2-value and bulk $B-V$ color is also found to be tight. Only a few S0 galaxies significantly deviate from the mean relation. The fact that the bulk of the stars in these S0's appears to be bluer than their central Mg_2-values can be explained by the presence of "blue" disks. In all other hot stellar systems the good correlation between bulk $B-V$ color and central Mg_2 shows that population gradients must be similar in all systems (a point made previously in Burstein et al. 1988b and which will be discussed in detail in Paper III of the present series).

3. The low scatter about the mean Mg_2–σ_0 relation implies that the *combined* relative variation of age *and* metallicity at a given velocity dispersion is of the order of only 15% (rms) for the bright objects and presumably much larger for the faintest systems. It is not very likely that *all* scatter is due to differences in three-dimensional shape.

4. The residuals from the mean Mg_2–σ_0 relation do not correlate with the distance of the galaxies *from* the fundamental plane nor with their position *within* the fundamental plane. They also do not correlate either with velocity dispersion anisotropy or isophotal shape. In the case of luminous ellipticals, the only known strong correlation is with structural peculiarities, as measured by the Schweizer et al. (1990) Σ-parameter. Another, but weaker, correlation may exist with the presence of peculiar core kinematics. While both effects can be naturally accounted for by spectral contamination of an old stellar population by a young stellar population formed in recent merger events, these spectroscopic anomalies per se are equally consistent with intrinsic metallicity variations

[3] Ironically, this means that the gaseous merger picture predicts, cum grano salis, a similar mechanism (i.e., infall of enriched material) to build up metallicity gradients as the standard dissipative formation picture of Larson (1975).

(Schweizer et al. 1990; Bertola, Burstein, & Buson 1993). For a handful of dwarf ellipticals and intermediate luminosity ellipticals, there is quite convincing evidence for a correlation of the Mg_2–σ_0 residuals with age—objects known to contain young or intermediate age stars have weak Mg_2 for their velocity dispersions (e.g., NGC 205, NGC 3156, NGC 4742).

5. To explain the observed tight relation between velocity dispersion and stellar population, we suggest a model in which the overall stellar population of a galaxy is determinined by a combination of total mass M and local density ρ: $P = f[(M^2\rho)^\gamma]$. It is envisioned that the mass constrains the ease with which metals can escape from the forming galaxies and the local density determines basic parameters of star formation, such as cooling, collapse, and star-formation time scale. The parameter γ and the ratio of the powers of M and ρ carry basic information about the star-formation process in dynamically hot galaxies—information that we have yet to fully understand. The tight Mg_2–σ_0 relation predicts $\gamma = 0.033$ if Mg_2 is used as the measure of differences in stellar populations.

The term "stellar population" is purposefully used here in a general way, as separation of age effects from metallicity effects remains problematic. Yet, the existence of *global* consistency suggests that stellar population variations *within* DHG galaxies are very systematic (e.g., Burstein et al. 1988b; Franx & Illingworth 1990). Paper III of this series will further explore these ideas.

Partial support for this research was provided by NSF grant AST-9016930 and NASA grant NAG5-547 (D. B.), DFG grant SFB328 (R. B.), and NSF grant AST-8702899 (S. M. F.). D. B. wishes to thank the hospitality of the Landessternwarte-Heidelberg. R. B. wishes to thank the hospitality of ASU.

REFERENCES

Aaronson, M., & Mould, J. R. 1985, ApJ, 290, 191
Bender, R. 1988a, A&A, 193, L7
———. 1988b, A&A, 202, L5
———. 1990, in Dynamics and Interactions of Galaxies, ed. R. Wielen (Berlin: Springer), 232
———. 1992, in IAU Symp. 149, The Stellar Populations of Galaxies, ed. B. Barbuy & A. Renzini (Dordrecht: Reidel), 267
Bender, R., Burstein, D., & Faber, S. M. 1992, ApJ, 399, 462 (B^2F1)
Bender, R., & Nieto, J.-L. 1990, A&A, 239, 79
Bender, R., Paquet, A., & Nieto, J.-L. 1991, A&A, 246, 349
Bender, R., & Surma, P. 1992, A&A, 258, 250
Bender, R., Surma, P., Döbereiner, S., Möllenhoff, C., & Madejsky, R. 1989, A&A, 217, 35
Bertola, F., Burstein, D., & Buson, L. M. 1993, ApJ, 403, 573
Binggeli, B. 1992, private communication
Binggeli, B., Sandage, A., & Tammann, G. A. 1985, AJ, 90, 1681
Binney, J., & Tremaine, S. 1987, Galactic Dynamics (Princeton: Princeton Univ. Press)
Bower, R. G., Lucey, J. R., & Ellis, R. S. 1992, MNRAS, 254, 589
Burstein, D. 1985, PASP, 97, 89
Burstein, D., Bertola, F., Buson, L. M., Faber, S. M., & Lauer, T. R. 1988a, ApJ, 328, 440
Burstein, D., Davies, R. L., Dressler, A., Faber, S. M., Lynden-Bell, D., Terlevich, R., & Wegner, G. 1988b, in Towards Understanding Galaxies at Large Redshift, ed. R. G. Kron & A. Renzini (Dordrecht: Kluwer)
Burstein, D., Davies, R. L., Dressler, A., Faber, S. M., Stone, R. P. S., Lynden-Bell, D., Terlevich, R., & Wegner, G. 1987, ApJS, 64, 601
Burstein, D., Faber, S. M., & Dressler, A. 1990, ApJ, 354, 18
Burstein, D., Faber, S. M., Gaskell, C. M., & Krumm, N. 1984, ApJ, 287, 586
Burstein, D., & Heiles, C. 1984, ApJS, 54, 33
Caldwell, N., Armandroff, T. E., Seitzer, P., & Da Costa, G. S. 1992, AJ, 103, 840
Charlot, S., & Bruzual, G. A. 1991, ApJ, 367, 126
Davies, R. L., & Birkinshaw, M. 1988, ApJS, 68, 409
Davies, R. L., Burstein, D., Dressler, A., Faber, S. M., Lynden-Bell, D., Terlevich, R. J., & Wegner, G. 1987, ApJS, 64, 581
Davies, R. L., Efstathiou, G., Fall, S. M., Illingworth, G. D., & Schechter, P. 1983, ApJ, 266, 41
Davies, R. L., & Illingworth, G. D. 1983, ApJ, 266, 516
Dekel, A., & Silk, J. 1986, ApJ, 303, 39
de Vaucouleurs, G., de Vaucouleurs, A., & Corwin, H. G., Jr. 1976, Second Reference Catalog of Bright Galaxies (Austin: Univ. Texas Press) (RC2)
de Vaucouleurs, G., de Vaucouleurs, A., Corwin, H. G., Jr., Buta, R. J., Paturel, G., & Fouqué, P. 1991, Third Reference Catalog of Bright Galaxies (NY: Springer) (RC3)
de Zeeuw, T., & Franx, M. 1991, ARA&A, 29, 239
Djorgovski, S., & Davis, M. 1987, ApJ, 313, 59
Dressler, A. 1984, ApJ, 281, 512
Dressler, A., Lynden-Bell, D., Burstein, D., Davies, R. L., Faber, S. M., Terlevich, R. J., & Wegner, G. 1987, ApJ, 313, 42
Edmunds, M. G. 1992, in IAU Symp. 149, The Stellar Populations of Galaxies, ed. B. Barbuy & A. Renzini (Dordrecht: Kluwer), 281
Efstathiou, G., & Gorgas, J. 1985, MNRAS, 239, 325
Ellis, R. S. 1992, in IAU Symp. 149, The Stellar Populations of Galaxies, ed. B. Barbuy & A. Renzini (Dordrecht: Kluwer), 297
Faber, S. M. 1973, ApJ, 179, 423
Faber, S. M., Dressler, A., Davies, R. L., Burstein, D., Lynden-Bell, D., Terlevich, R., & Wegner, G. 1987, in Nearly Normal Galaxies, from the Planck Time to the Present, ed. S. M. Faber (NY: Springer), 175
Faber, S. M., Friel, E. D., Burstein, D., & Gaskell, C. M. 1985, ApJS, 57, 711
Faber, S. M., Wegner, G., Burstein, D., Davies, R. L., Dressler, A., Lynden-Bell, D., & Terlevich, R. J. 1989, ApJS, 69, 763
Faber, S. M., Worthey, G., & Gonzalez, J. J. 1992, in IAU Symp. 149, The Stellar Populations of Galaxies, ed. B. Barbuy & A. Renzini (Dordrecht: Kluwer), 255
Franx, M., & Illingworth, G. 1988, ApJ, 327, L55
———. 1990, ApJ, 359, L41
Franx, M., Illingworth, G., & Heckman, T. M. 1989, ApJ, 344, 613
Freedman, W. L. 1992, in IAU Symp. 149, The Stellar Populations of Galaxies, ed. B. Barbuy & A. Renzini (Dordrecht: Kluwer), 169
Freeman, K. C. 1987, in Nearly Normal Galaxies, From the Planck Time to the Present, ed. S. M. Faber (NY: Springer), 317
Frogel, J. A. 1988, in Towards Understanding Galaxies at Large Redshift, ed. R. G. Kron & A. Renzini (Dordrecht: Kluwer), 1
Gorgas, J., Efstathiou, G., & Aragon Salamanca, A. 1990, MNRAS, 245, 217
Gregg, M. G. 1989, ApJ, 337, 45
———. 1992, ApJ, 384, 43
Hernquist, L., & Barnes, J. 1991, Nature, 354, 210
Hodge, P. 1989, ARA&A, 27, 139
Jedrzejewski, R. I., & Schechter, P. L. 1988, ApJ, 330, L87
Kent, S. M. 1985, ApJS, 59, 115
———. 1987, AJ, 94, 306
Kormendy, J., & Illingworth, G. 1982, ApJ, 256, 460
Kormendy, J., & Sanders, D. B. 1992, ApJ, 390, L53
Larson, R. B. 1974, MNRAS, 169, 221
———. 1975, MNRAS, 173, 671
Mateo, M., Olszewski, E., Welch, D. L., Fischer, P., & Kunkel, W. 1991, AJ, 102, 914
Mould, J. R. 1978, ApJ, 220, 434
O'Connell, R. W. 1980, ApJ, 236, 430
———. 1986, in Stellar Populations, ed. C. Norman et al. (Cambridge: Cambridge Univ. Press), 167
Paltoglou, G., & Freeman, K. C. 1987, in IAU Symp. 127, Structure and Dynamics of Elliptical Galaxies, ed. T. de Zeeuw (Dordrecht: Reidel), 447
Paquet, A., Bender, R., & Seifert, W. 1992, in IAU Symp. 149, The Stellar Populations of Galaxies, ed. B. Barbuy & A. Renzini (Dordrecht: Kluwer), 466
———. 1993, in preparation
Peletier, R. 1990, Ph.D. thesis, Univ. Groningen
Prugniel, P. 1989, Ph.D. thesis, Univ. Paul Sabatier, Toulouse
Renzini, A. 1986, in Stellar Populations, ed. C. Norman et al. (Cambridge: Cambridge Univ. Press), 213
Rich, R. M., & Mould, J. 1991, AJ, 101, 1286
Rose, J. A. 1985, AJ, 90, 1927
Sandage, A., & Tammann, G. A. 1981, A Revised Shapley-Ames Catalog of Bright Galaxies (Washington, DC: Carnegie Inst. Washington)
Sandage, A., & Visvanathan, N. 1978, ApJ, 223, 707
Schechter, P. L., & Gunn, J. E. 1979, ApJ, 229, 472
Schweizer, F. 1990, in Dynamics and Interactions of Galaxies, ed. R. Wielen (Berlin: Springer), 60
Schweizer, F., & Seitzer, P. 1993, AJ, 104, in press
Schweizer, F., Seitzer, P., Faber, S. M., Burstein, D., Dalle Ore, C. M., & Gonzalez, J. J. 1990, ApJ, 364, L33
Seifert, W. 1990, Ph.D. thesis, Univ. Heidelberg
Silk, J. 1992, in IAU Symp. 149, The Stellar Populations of Galaxies, ed. B. Barbuy & A. Renzini (Dordrecht: Kluwer), 367
Sulentic, J. W., & Tifft, W. G. 1973, The Revised General Catalogue of Non-stellar Astronomical Objects (Tucson: Univ. Arizona Press) (RNGC)

Terlevich, R., Davies, R. L., Faber, S. M., & Burstein, D. 1981, MNRAS, 196, 381
Terndrup, D. M. 1988, AJ, 96, 884
Thomsen, B., & Baum, W. A. 1989, ApJ, 347, 214
Tonry, J. L. 1984, ApJ, 283, L27
Vader, J. P. 1987, ApJ, 317, 128
van den Bergh, S. 1972, in IAU Symp. 44, External Galaxies and Quasi-Stellar Objects (Dordrecht: Reidel), 1
———. 1986, AJ, 91, 271
Whitmore, B. C., McElroy, D. B., & Tonry, J. L. 1985, ApJS, 59, 1
Yoshii, Y., & Arimoto, N. 1987, A&A, 188, 13
Zinn, R. 1985, Mem. Soc. Astron. Ital., 56, 223